Texas A&M University
Mechanical Engineering Department
Turbomachinery Laboratory
Tribology Group

RESPONSE OF AN OPEN ENDS SQUEEZE FILM DAMPER TO SERIES OF CONSECUTIVE IMPACT LOADS

Research Progress Report to the TAMU Turbomachinery Research Consortium

TRC-SFD-01-2015

by

Luis San Andrés
Mast-Childs Chair Professor
Principal Investigator

Sung-Hwa Jeung
Research Assistant

Scott Tran
UG student worker

May 2015

EXECUTIVE SUMMARY

RESPONSE OF AN OPEN ENDS SQUEEZE FILM DAMPER TO SERIES OF CONSECUTIVE IMPACT LOADS

LUIS SAN ANDRÉS, SUNG-HWA JEUNG, & SCOTT TRAN

Aircraft gas turbine engines require of appropriate means to control rotor vibration while ensuring structural isolation. Squeeze Film Dampers (SFDs) serve to mitigate rotor vibration amplitudes and control instability in rotor-bearing systems. SFDs, however, are custom made to provide the desired level of damping. The 2015 TRC report details progress on the experiments performed with a short length (L/D=0.2) open ends SFD with a film land length L=25.4 mm (1 in), diameter D=127 mm (5 in), and radial clearance c=267 μm (10.5 mil). The measurements quantify the SFD transient response to impact loads for motions starting at static eccentricity e_s/c=0 to 0.6. The tests refer to single impacts, two or more consecutive impacts with an elapsed time of 30 ms in between successive impacts, and two or more consecutive impacts -without any delay between them- and with a load magnitude at 50% of the preceding (impact) load amplitude.

The identified damping ratio (ζ) increases both with the BC amplitude (Z_{MAX}, i.e. the load magnitude, and the initial static eccentricity e_s. For an identical damper having a smaller clearance c_s=0.213 mm, ζ is ~1.3 to ~1.7 times greater than the damping ratio for the current damper which has a 25% larger film clearance. Since $\zeta \sim C/M$ is proportional to the damping coefficient (C) over the inertia coefficient (M), the damping ratio (ζ) scales approximately with the square of the film clearance, i.e., $\zeta \sim 1/c^2$.

The transient responses recorded for a series of consecutive impacts with an elapsed time between impacts of 30 ms (T_i=30 ms) shows an increase of the peak BC amplitude (Z_{MAX}). For the transient response due to consecutive impacts, one after the other (*with no delay*), the external force acts as an impulse adding (positive) BC velocity to the system and thus increasing the following BC peak amplitude(Z_{MAX}). The BC amplitude also increases with the amplitude of impact load and for motions departing from a more off-centered position (e_s).

A physically unsound variability in peak or maximum BC amplitude versus the number of impacts applied is unexplained and to be addressed in the future.

Nomenclature

a_X,a_Y	Journal center acceleration along X and Y directions [m/s^2]
c	Nominal radial clearance [m]
D	Journal diameter [m], R= ½ D
e_s	Static eccentricity (along 45^o) [m]
F	Impact load [N]
f_n	Test system Natural frequency [Hz]
h	Lubricant film thickness [mm]
K_S	Structural support stiffness [N/m]
L	Film land length [m]
M_{SFD}	Squeeze Film Damper mass [kg]
M_{BC}	Bearing cartridge mass [kg]
N	Number of periods of motion [-]
N	Number of impacts [-]
P	Dynamic film pressures [Pa]
P_I	Pressure induced by fluid inertial effect [Pa]
P_{in}	Static oil pressure at journal inlet [Pa]
P_V	Pressure induced by fluid viscous effect [Pa]
Q_{in}	Lubricant flow rate [LPM]
T	Time [s]
T	Temperature [℃]
T_i	Elapsed time between impacts [s]
T_{IMP}	Duration of impact [s]
V_X, V_Y	Journal center velocity along X and Y directions [m/s]
X,Y	Coordinate axes
Z	Bearing cartridge maximum displacement [m]
e_s/c	Dimensionless eccentricity [-]
ξ	Damping ratio [-]
δ	Logarithmic decrement ($2\pi\xi/\sqrt{1-\xi^2}$) [-]
ρ, μ	Oil density [kg/m^3] and viscosity [Pa.s]
ϕ	Feed hole diameter [mm]

Subscripts

BC	Bearing cartridge
s	Structure
L	Lubricated system
SFD	Squeeze film damper

TABLE OF CONTENTS

RESPONSE OF AN OPEN ENDS SQUEEZE FILM DAMPER TO SERIES OF CONSECUTIVE IMPACT LOADS

LUIS SAN ANDRÉS, SUNG-HWA JEUNG, & SCOTT TRAN
MAY 2015

page

EXECUTIVE SUMMARY ii

NOMENCLATURE iii

LIST OF TABLES v

LIST OF FIGURES v

Introduction 1

Test rig description 4

Single Impact Load Tests 7

- Experimental Procedure 7
- Identification of Logarithmic Decrement and Damped Natural Frequency of Lubricated Damper System[1] 11

Series of Consecutive Impact Load Tests 17

- Consecutive Impacts with Equal Load Magnitude 17
- Transient Response Characteristics 20
- System Transient Response to a Series of Impacts of Varying Load Amplitude 24

Prediction of Transient Response for the Test System 31

- Predicted Transient Response Characteristics 32

Conclusion and Recommendations 34

Acknowledgement 35

References 35

APPENDIX A. Identification of (Dry) Test System Structure Parameters 38

APPENDIX B. Measurement of test damper clearance 41

APPENDIX C. Measurement of Lubricant Properties and Flow Rate 43

APPENDIX D. Recorded Film Pressures in Test SFD 47

APPENDIX E. Maximum displacement versus peak amplitude of impact loads 53

APPENDIX F. Predicted Transient Response 56

LIST OF TABLES

No		page
1	Main features of test damper	6
2	Operating conditions for test damper (Inlet flow rate Q_{in}=5 LPM, static inlet pressure P_{in}=0.34 bar(g)).	8
3	SFD configuration and operating conditions for two film clearances	15
4	Operating conditions for test damper excited with repeated impact loads of equal magnitude. (Inlet flow rate Q_{in}=5 LPM, static inlet pressure P_{in}=0.34 bar(g), static eccentricity e_s=0).	17
5	Operating conditions for test damper with multiple impacts of decaying force amplitude. (Inlet flow rate Q_{in}=5 LPM, static inlet pressure P_{in}=0.34 bar(g)).	24
6	Physical parameters for prediction of forces for short-length open ends SFD.	32
B.1	Journal outer and BC inner diameter measured at three axial planes and three radial lines	42
C.1	Mobil Velocite™ No 3 (ISO VG 2) Manufacturer specification [C1]	43
C.2	Open ends SFD (c=0.267 mm) with hex socket orifice, ϕ=2.54 mm. Measured inlet pressures and lubricant flow rates. ISO VG 2 oil at room temperature T_S=23℃ [C2].	45

LIST OF FIGURES

No		page
1	(a) Photograph of the SFD test rig with shakers, static loader, and oil supply line (inset shows view from the top) and (b) cross section view of test SFD with physical dimensions and lubricant flow path (L=25.4 mm, D=126.7 mm, c=0.267 mm).	5
2	Journal with three orifices ϕ=2.5 mm, 120° apart. Film land length, L = 25.4 mm, D = 126.7 mm (L/D=0.2).	6
3	Schematic view of BC displaced relative to a stationary journal (Exaggerated film clearance for illustrative purpose).	7
4	Typical impact load along X direction and BC displacement $Z_{X(t)}$ versus time. Amplitude of DFT for Z_X shown.	9
5	Maximum displacement $\lvert Z_{MAX}\rvert_{X,Y}/c$ vs. peak amplitude of single impact load $F_{MAX}/(LD)$ for motions initiating from static eccentricity e_s/c=0.0, 0.2, 0.4, and	10

0.6. Open ends SFD with clearance c=0.267 mm.

6 Peak BC dynamic amplitude Z_{MAX}/c and damping envelope ($e^{-\xi\omega_n t}$) versus time (t). Measurements for $F_{MAX}/(LD)$=2.5 bar & 6.1 bar for motions from e_s/c=0, and for $F_{MAX}/(LD)$=5.4 bar for displacements from e_s/c=0.6. Amplitude of DFT for Z_X also shown. 13

7 System damping ratio (ζ) and logarithmic decrement (δ) vs. peak displacement (Z_{MAX}/c). Data for one impact load and motions departing from various static eccentricity. Open-ends SFD with c=0.267 mm and 25.4 mm length film land. 14

8 SFD damping ratio (ζ) versus peak BC (Z_{MAX}/c) displacement. Open-ends SFD with c=267 μm and c_s=213 μm [21]. L= 25.4 mm. Parameters identified for motions initiating at static eccentricity e_s/c=0. 16

9 (a) Sets of repeated (2-6) impact loads F(t) and (b) ensuing BC displacement Z(t) vs. time. Measurements for $F_{MAX\text{-}X}/(LD)$~3.1 bar and motions initiating from static eccentricity e_s/c=0. Average elapsed time between impacts T_i =~30 ms. 19

10 Maximum displacement $|Z_{MAX}|_{X,Y}/c$ vs. peak amplitude of unit load $F_{MAX}/(LD)$ for motions from centered condition (e_s/c=0.0). Data from two and three consecutive impacts with elapsed time between impacts T_i~30ms. Open ends SFD clearance c=0.267 mm (Insets show time traces of impact load and ensuing BC displacement). 21

11 Peak displacement $|Z|_{MAX}/c$ over peak amplitude of unit load $F_{MAX}/(LD)$ vs. number of impacts for motions initiating from the centered condition (e_s/c=0.0). Tests with increasing number of impacts from one to six. Average elapsed time between impacts T_i =~30 ms. (Open ends SFD clearance c=0.267 mm). 22

12 Normalized (a) BC displacement and velocity, and (b) velocity and impact loads vs. time for motions from e_s/c=0. Graphs shows data for six impacts (F_{MAX}=672 N). Elapsed time between impacts is T_i=~30 ms. 23

13(A) Impact load F(t) and ensuing BC displacement Z(t) versus time for (a) Case 1: single impact, (b) Case 3: three consecutive impacts, and (c) Case 4: four consecutive impacts. Measurements for $F_{MAX}/(LD)$=1.9 bar and motions departing from static eccentricity e_s/c=0. 26

13(B) Impact load F(t) and ensuing BC displacement Z(t) versus time for (a) Case 1: single impact, (b) Case 3: three consecutive impacts, and (c) Case 4: four consecutive impacts. Measurements for $F_{MAX}/(LD)$=7.9 bar and motions departing from static eccentricity e_s/c=0. 27

14	Normalized velocity and impact load and BC displacement and velocity vs. time for motions from e_s/c=0. Graphs shows data for four consecutive impacts for (a) F_{MAX}=992 N and (b) F_{MAX}=2,540 N. Elapsed time between impacts is T_i=~0 ms.	28
15	Ensuing maximum BC displacement $\|Z_{MAX}\|_{X,Y}$/c versus peak unit load $F_{MAX}/(LD)$ for BC motions initiating from e_s/c=0.0, 0.2, 0.4, and 0.6. Tests with one, three and four consecutive impacts; elapsed time between impacts T_i=0 ms. (Open ends SFD nominal clearance c=267 μm.)	29
16	Peak displacement $\|Z_{X,Y}\|_{MAX}/c$ over peak amplitude of unit load $F_{MAX}/(LD)$ vs. static eccentricity (e_s/c). Tests with three and four consecutive impacts; elapsed time between impacts T_i=0 ms. Open ends SFD clearance c=0.267 mm.	30
17	Comparison of experimental and predicted BC peak displacements $\|Z_{X,Y}\|_{MAX}/c$ over peak amplitude of unit load $F_{MAX}/(LD)$ vs. number of consecutive impacts for motions from e_s/c=0. Duration of impact T_{IMP}=1.4 ms and time between impacts T_i=30 ms.	33
A.1	(a) Schematic view of static load test setup and (b) static load versus BC displacement and estimated structural stiffness along the X, Y axes and along the 45° direction.	38
A.2	Dimensionless BC acceleration (ā) and DFT of its amplitude for ā versus time (t). Measurements for along the X, Y directions and 45° away at centered condition (e_s=0).	40
B.1	Measurement planes for journal outer diameter (D planes are radial lines with constant spacing of 60°, section A-A shows axial planes spaced 12.7 mm (0.5 in) apart).	41
C.1	Measured lubricant viscosity versus temperature. Viscosity measured with a rotary viscometer.	44
C.2	Measured flow rate versus inlet pressure for journal with hex socket orifices ϕ=2.54 mm.	45
D.1	Schematic views of the disposition of pressure sensors in the BC: (a) top view, (b) axial view and (c) unwrapped view [21].	48
D.2	Dynamic film pressures ($P4$) and film thickness (h) recorded at the mid-plane (z=0), and location of minimum film thickness for four static eccentricities. Unidirectional load along Y direction, $F_{MAX}/(LD)$=3.9 bar.	49

D.3 Recorded peak film dynamic pressure versus maximum unit load $F_{MAX}/(LD)$ of single impact for motions from centered condition e_s/c=0 and three static eccentricity e_s/c=0.2, 0.4, and 0.6. Measurements at damper mid-plane, top and bottom half-planes. (Insets show location of pressure sensors along film land, and show journal position relative to the BC). 51

E.1 Maximum displacement $|Z_{MAX}|_{X,Y}/c$ vs. peak amplitude of unit load $F_{MAX}/(LD)$ for motions from e_s/c=0 for four consecutive impact loads. Elapsed time between impacts T_i~30ms. Averaged over 20 test sets. Open ends SFD clearance c=0.267 mm. (Insets show time traces of impact load and ensuing BC displacement). 54

E.2 Maximum displacement $|Z_{MAX}|_{X,Y}/c$ vs. peak amplitude of unit load $F_{MAX}/(LD)$ for motions from e_s/c=0 for six consecutive impact loads Elapsed time between impacts T_i~30ms. Averaged over 20 test sets. Open ends SFD clearance c=0.267 mm. (Insets show time traces of impact load and ensuing BC displacement). 55

F.1 Predictions: (a) Seven consecutive impact load F(t) and (b) calculated journal displacement Z(t) versus time. $F_{MAX\text{-}X}/(LD)$= 3.1 bar and motions from e_s/c=0. Elapsed time between impact T_i =~30 ms. 57

F.2 Predicted maximum displacement $|Z_{MAX}|_{X,Y}/c$ vs. peak amplitude of impact load $F_{MAX}/(LD)$ for motions from e_s/c=0. 58

Introduction

High performance turbomachinery uses advanced materials and manufacturing techniques, demands operation at high shaft speeds to increase power, and requires of larger tolerance to rotor imbalance and tighter clearances in (secondary) flow passages. Squeeze Film dampers (SFDs) aid to reduce rotor vibrations due to imbalance and other sources, and also isolate a rotor from the engine frame or casing [1,2].

Compact aircraft gas turbines customarily implement ultra-short length SFDs ($L/D \leq 0.2$) where overall weight and space are at a premium. These engines need to endure sudden shock loads during hard landings and takeoffs. In large size grinding machines, SFDs serve as cushions that quickly dissipate mechanical energy from sudden plunging motions when the tool contacts intermittently with the working piece. These transient events, characterized by large journal center speed and acceleration/deceleration rates, produce large amplitude forces that may affect the integrity of the mechanical elements and could even lead to system failure. Adequate damping to ameliorate rotor vibrations is paramount to ensure system reliability. Reliable rotor dynamic operation of turbomachinery calls for a detailed characterization of SFD forced performance under stringent operating conditions.

The measurement of the forced performance of an actual bearing configuration is most reliable to validate engineering products and to establish a sound mechanical design process. Prediction of SFD forced performance customarily derived from linearized analyses is valid for small amplitude motions about the journal center condition ($e=0$). Hence, it is not surprising then that many research efforts [3-5] concentrate on experimentally estimating the forced performance of SFDs subject to large amplitude motions, in particular circular orbit motions. However, a number of operating conditions do not lead to circular synchronous precession of a SFD journal; for example, hard landings and blade loss events. Hence, an engine manufacturer has a need to certify system and components' performance under large sudden transient loads.

To evaluate the feasibility of a thin film journal bearing design, Gunter *et al*. [6,7] pioneered the nonlinear transient response analysis of a simple rigid rotor supported on open ends, short length SFDs, and to predict the maximum force transmitted through the support structure. The authors note that under blade loss events, a time-transient analysis

of the SFD is adequate to predict the forced performance that could affect the integrity of the bearing support.

Later, Stallone *et al*. [8] deliver analyses that characterize the transient nonlinear response of an aero-engine experiencing a blade loss event, further validating predictions against experimental data. A blade loss leads to rapid changes in acceleration/deceleration rates of a journal, which causes large transmitted forces to the rotor-bearing support. Sun *et al*. [9,10] and Zhang *et al*. [11,12] performed similar computational studies to analyze the transient response of a point mass-SFD and to validate the reduction in transmitted force by providing viscous damping. Refs. [9,10] note that with an increasing rotor system imbalance due to blade loss, the power loss due to viscous dissipation in a SFD increases. Zhang *et al.* [11,12] present a time transient simulation showing that blade loss events could lead to a large transmissibility (T>1), rendering the SFD ineffective. Refs. [9-12], however, do not include comparisons with experimental results or with field data.

Walton and Heshmat [13] simulate blade loss event transient response tests for a rotor supported on sealed ends SFD. The experimental program shows that with an increase in *unbalance forces*, the peak-to-peak amplitude of the journal motion increases, and thus results in a large transmitted force that can lead to bearing failure. However, increasing the oil supply pressure into the damper, from 3.4 bar to 5.5 bar, causes the rotor amplitude to reduce even for a large mass imbalance test case.

By applying the transient response technique, Ishii and Kirk [14] determine the optimum support damping for a catcher bearing that protects an active magnetic bearing (AMB) in case of failure. Later, Sun and Palazzolo [15,16] present results on the transient response of a simple rotor-catcher bearing system including a squeeze film damper on the outer race of the bearing. These works describe the thermal effect on the catcher-bearing surface when the rotor drops in case of an AMB failure. The results highlight the importance of the optimal damping in a SFD, which serves to minimize temperature increase in the catcher bearing, and thus extends its life.

Roberts *et al*. [17-19] use a linear model of the squeeze-film to determine the SFD force coefficients, damping and inertia, from the experimental data of a freely decaying transient response experimental data. The damping and inertial coefficients are validated

against the predictions and found to be independent of the frequency of excitation when all other variables (c, e_s, L) are kept constant.

Lee *et al*. [20] demonstrate both analytically and experimentally that the transient response of a rotor-bearing system is sensitive to the time duration of the external shocks, i.e., the larger the duration of the shock, the larger the rotor amplitude will have. San Andrés and Jeung [21], 2014 TRC Annual Progress Report, present measurements of the transient response of an open ends SFD test rig due to an impact load of increasing amplitude ($F_{MAX}/(LD)$=1.5 – 10 bar). The impact load tests intend to reproduce operation of a rotor-bearing system incorporating SFD experiencing a hard landing. The test results show that the SFD direct damping and inertia force coefficients increase rapidly with an increasing peak amplitude of dynamic motion, in particular for those due to the impact load with largest magnitude. In spite of the rapid growth in damping (C) coefficients, an increasing amplitude of dynamic motion does not lead to a significant increase in damping ratio due to a large increase in the inertia (M) coefficient since $\xi \sim C/M$. Further, Ref. [22] distils the contents presented in Ref. [21].

From the reviewed literature, only a handful of Refs. [13,20-22] attempt an experimental evaluation of the SFD forced performance enduring large journal amplitude motions due to sudden maneuver loads.

This report further evaluates the dynamic forced performance of an ultra-short (L/D=0.2) open ends SFD test rig from an external impact (intermittent) load which causes a peak journal amplitude as large as 60% of the radial clearance for motions departing from a static eccentricity e_s/c=0, 0.2, 0.4, and 0.6. The report includes the identification of the logarithmic decrement and damped natural frequency for the lubricated test SFD system, the assessment of the transient response characteristics and recorded film dynamic pressures, and comparisons with predictions from a short length open ends SFD model. The present work intends to give a more comprehensive assessment of a SFD subject to a sudden impulsive load that produces transient displacements spanning from small to large amplitudes.

Test Rig Description

Figure 1 shows a photograph of the current SFD test rig with its major components labeled and Table 1 lists the current damper geometry. Annual progress report TRC-SFD-01-2014 [21] details the test rig description. Two electromagnetic shakers (e-shakers) are positioned orthogonally along the noted *X* and *Y* axes. A static loader positioned halfway between the two shakers, 45° away, applies a static load to displace the test bearing to a desired static eccentricity (e_s).

The SFD test bearing consists of a test journal mounted on a journal base, rigidly fastened to a pedestal bolted into a cast iron table. The feature allows the test journal to be exchangeable without disturbing the instrumentation set up. The film land consists of the annular gap between the outer surface of the test journal and the inner circumference of the bearing cartridge (BC).

Flexural rods make the support structure of the BC that replicates a squirrel cage support. The structural stiffness can increase or decrease by varying the number of installed rods. Presently, four structural rods (90° apart) support the BC with mass M_{BC}=15.15 kg. In Figure (b), an inset (top view) shows the position of the rods with respect to *X* and *Y* axes. The rods provide a structural stiffness K_S~9.0 MN/m and ensure the BC is properly aligned and centered. **Appendix A** details the identification of the rods' structural stiffness (K_S).

Figure 2 depicts a journal and BC used in the experiments that consists of a single land damper with a journal diameter *D*=127 mm (5 inch), film land length *L*= 25.4 mm (1 inch), and a nominal radial clearance *c*=267 μm (10.5 mil). **Appendix B** presents the physical dimensions of the machined test journal. Lubricant flows into the film land through three feedholes, 120° apart, machined in the journal. The design enables the size of the (active) lubricant feedholes to vary by inserting hex socket screws into the feedholes. In the current configuration, the orifices have a diameter ϕ = 2.5 mm (0.1 in). Ref. [4] gives details on the lubricant flow path thru the system components.

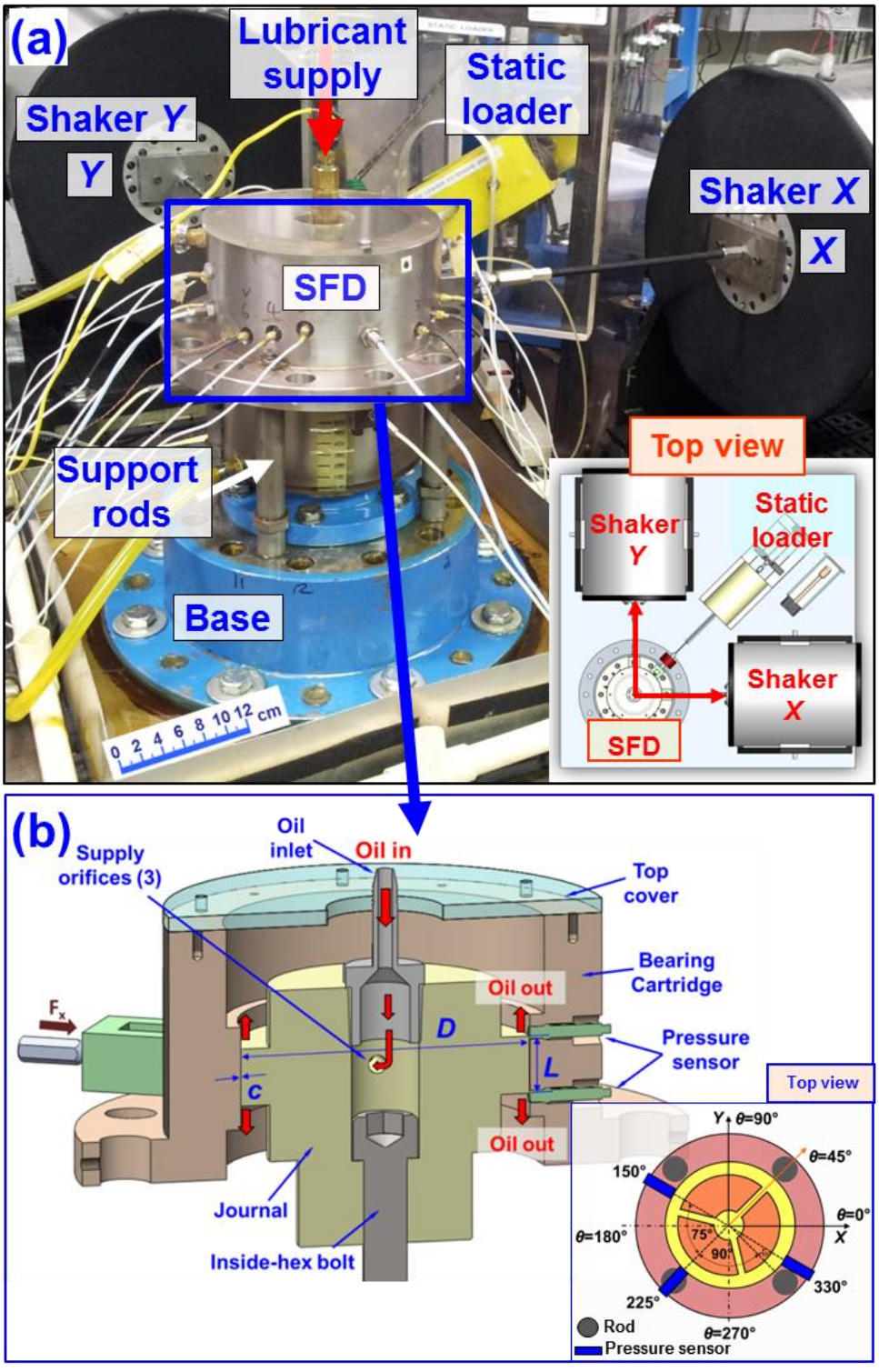

Figure 1. (a) Photograph of the SFD test rig with shakers, static loader, and oil supply line (inset shows view from the top) and (b) cross section view of test SFD with physical dimensions and lubricant flow path (*L*=25.4 mm, *D*=126.7 mm, *c*=0.267 mm).

Table 1. Main features of test damper

Single film land length, L (mm)	Journal Diameter, D (mm)	Radial clearance, c (μm)	Feedhole diameter, ϕ (mm)	Structural stiffness, K_S (MN/m)	Active Feedholes	Ends condition
25.4	127	267	2.5	9.0	3	Open

The oil used is an ISO VG2, a light lubricant with a rated density and kinematic viscosity comparable to those of lubricants used in aircraft engines operating at a high temperature. The measured viscosity is μ=0.384 micro-Reyns (2.65 cP) and density is ρ=799.3 kg/m^3 (49.9 lb/ft^3) at temperature T_S=73°F (23°C). **Appendix C** details the measured lubricant viscosity versus temperature and the estimated flow conductance through the film lands.

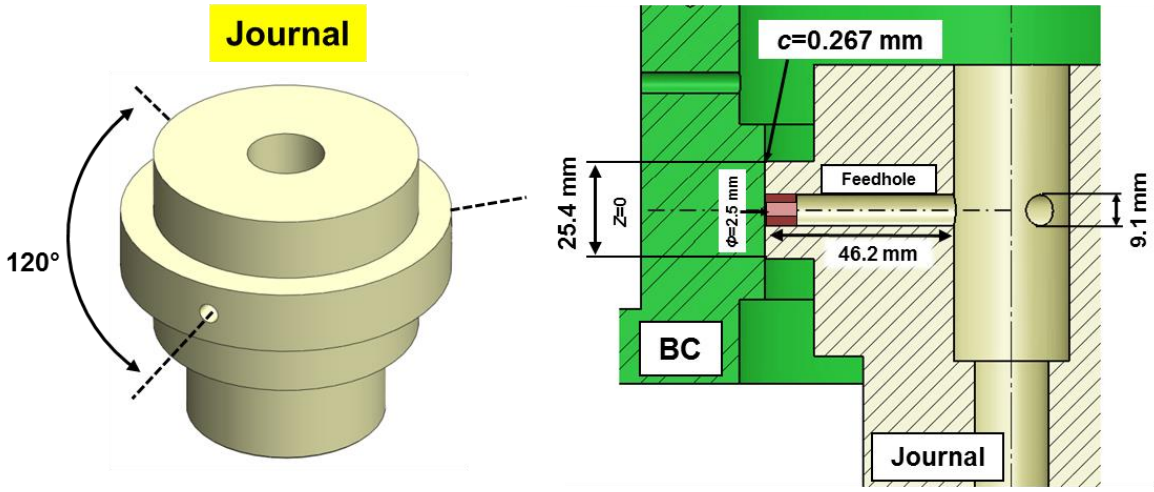

Figure 2. Journal with three orifices ϕ=2.5 mm, 120° apart. Film land length, L = 25.4 mm, D = 126.7 mm. (L/D=0.2).

Single Impact Load Tests

Experimental Procedure

Figure 3 displays a schematic view of the BC at a statically off-centered condition. The static loader pulls the bearing cartridge to a desired static eccentricity (e_s), 45° away from the X and Y directions. Note the BC displaces relative to the fixed journal. With an increasing static eccentricity e_s, the damper clearance at Θ=225° decreases; this is the location of the minimum clearance.

Sets of single impact load tests are exerted to quantify the effect of a sudden load on the SFD transient response departing from e_s=0.0c, 0.2c, 0.4c, 0.6c. One end of the stinger attaches to the shaker, while the other end is free, i.e., not fastened to the load cell mounted on the BC. The stinger displaces 0.254 mm (1/10 inch) before hitting the BC.

An impact load acts to displace the BC away from the (stationary) journal; hence at the incidence of an impact, either in the X or Y directions; the local film thickness at Θ=225° will begin to increase (see Fig. 3).

The following figures present the measured peak BC displacement Z_{MAX} including both the static and dynamic displacements that is,

$$Z_{MAX} = Z_{STAT} + Z_{DYN}(t) \qquad (1)$$

Note the static displacement both along the X and Y directions is $Z_{STAT} = (e_s/c)\cos(45^o)$.

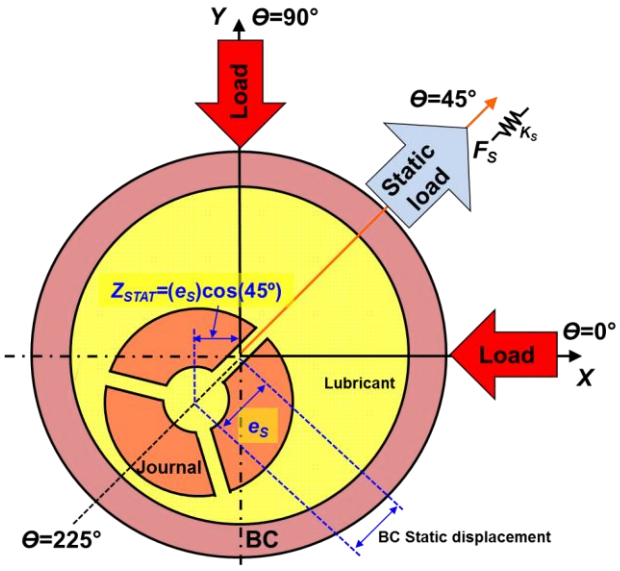

Figure 3 Schematic view of BC displaced relative to a stationary journal. (Exaggerated film clearance for illustrative purpose)**.**

Table 2 depicts operating conditions for the tests performed on the open end SFD with a radial clearance c=0.267 mm. In each set, twenty single impact loads are delivered along the X direction, while no load is imposed on the BC along the Y axis. Later, identical tests follow with impact loads along the Y-direction. The load sets include forces with a peak magnitude from 0.5 kN to 2.5 kN ($F_{MAX}/(LD)$=1.5 – 7.8 bar).

The shaker controller/DAQ LabVIEW® program records the test system dynamic time response (F_X, F_Y, Z_X, Z_Y, a_X, a_Y) at a rate of 16,384 samples/s during a time span of 0.25 s.

Table 2 Operating conditions for test damper (Inlet flow rate Q_{in}=5 LPM, static inlet pressure P_{in}=0.34 bar(g)).

Radial clearance, c (μm)	Motion type	Average of # test sets	Impact duration (s)	External load, F_{MAX} (N)	$F_{MAX}/(LD)$ (bar)	Static eccentricity, e_s/c
267	Unidirectional single impact load	20	1.4	500	1.5	**0.0, 0.2, 0.4, 0.6**
				750	2.3	
				1000	3.1	
				1500	4.7	
				2000	6.2	
				2500	7.8	

Figure 4 depicts the time trace of a typical impact load delivered to the BC along the X direction and the ensuing BC displacement (Z_X). The impact load has a peak amplitude $F_{MAX\text{-}X}$=0.8 kN and the maximum BC amplitude $|Z_X|_{MAX}$ =0.17c. The impact load, resembling a sharp half-sine wave, lasts ~ Δt_{IMP}= 1.4 ms. The response of the BC is characterized as oscillatory, with an exponentially decaying amplitude, lasting ~ 0.25 s. A frequency analysis of the BC response shows motion with two distinct natural frequencies of the test rig, ω_{n1}=124 Hz and ω_{n2}=188 Hz, as shown in the amplitude of the DFT (discrete Fourier transform) for the displacement Z_X. The BC displacement Y, orthogonal to the direction of the impact load, is negligible and not shown for brevity.

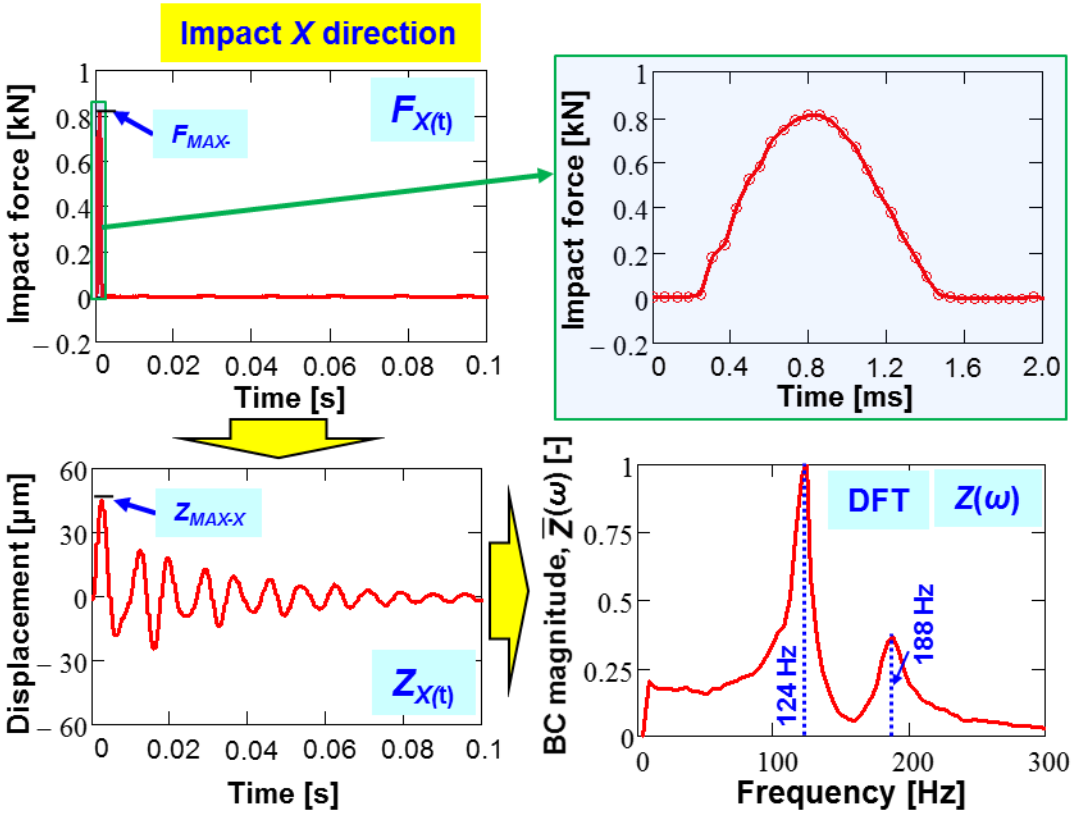

Figure 4. Typical impact load along *X* direction and BC dynamic displacement Z_X versus time. Amplitude of DFT for Z_X shown.

Figure 5 depicts the maximum BC displacement ($|Z_{X,Y}|_{MAX}/c$) vs. the peak amplitude of the impact load ($F_{MAX}/(LD)$) applied along the *X* or *Y* directions for motions initiating from static eccentricity e_s/c=0.0, 0.2, 0.4, and 0.6. Each data point represents the average of responses collected over 20 impacts, *i.e.*

$$\frac{1}{n}\sum_{i=1}^{n}\left[\frac{Z_{MAX}/c}{F_{MAX}/(LD)}\right]_i \qquad (2)$$

The dash lines show a simple linear curve fit, which for most conditions evidences a linear relationship between the peak BC displacement and peak impact load $(Z_{MAX}/c)/(F_{MAX}/(LD))$. A large load displaces the BC with a large (dynamic) amplitude. However, increasing the static eccentricity (e_s/c) shows no significant difference in the slope of $(Z/F)_{MAX}$.

Note, later in Figures 11 and 16, for motions starting at an increasing static eccentricity, the slope of the line fit to Z_{MAX} vs. F_{MAX} for a single impact is compared against those slopes for the transient response due to a series of consecutive impacts.

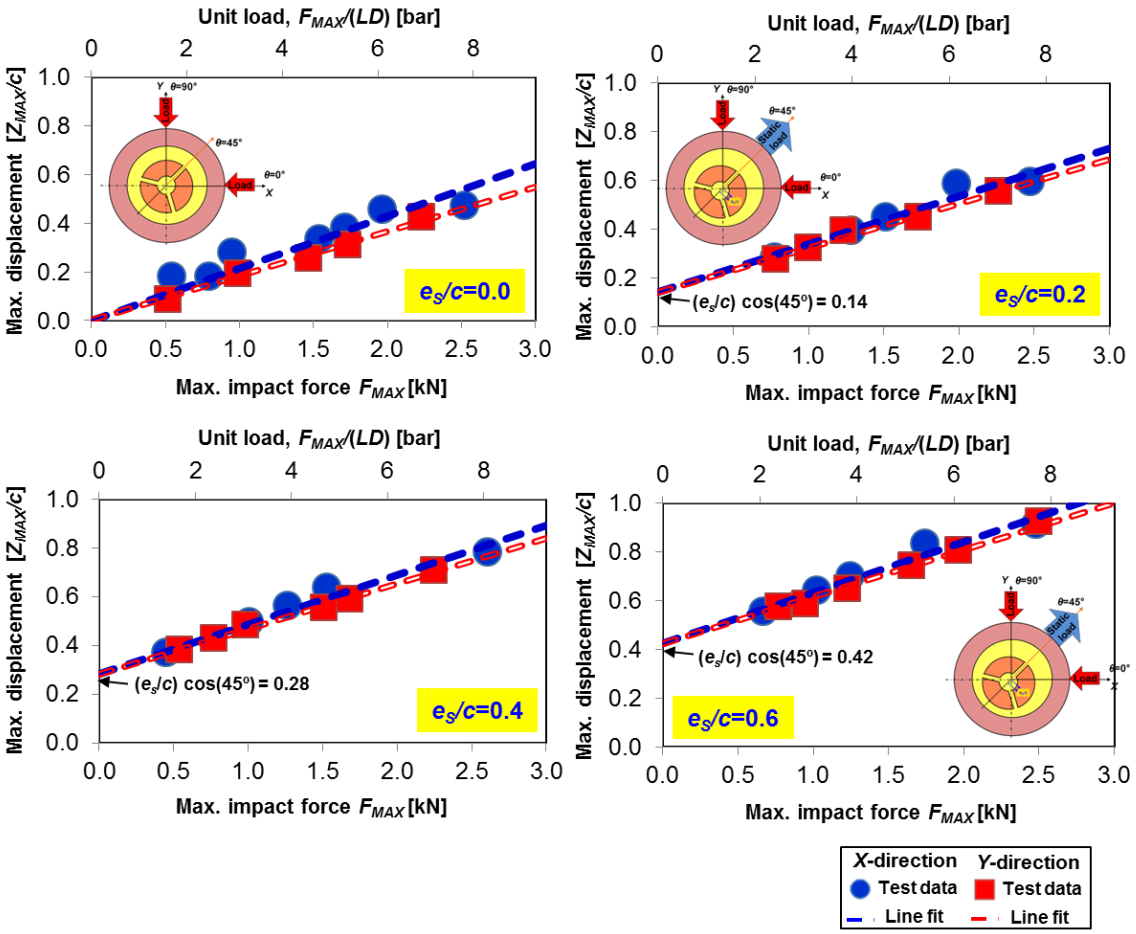

Figure 5. Maximum displacement $|Z_{MAX}|_{X,Y}/c$ vs. peak amplitude of single impact load $F_{MAX}/(LD)$ for motions initiating from static eccentricity e_s/c=0.0, 0.2, 0.4, and 0.6. Open ends SFD with clearance c=0.267 mm.

Identification of Logarithmic Decrement and Damped Natural Frequency of Lubricated Damper System[1]

As shown in Figure 4, the BC response to an external impact decays exponentially, typical of a viscous under-damped system. Hence, the recorded response leads to the identification of the system logarithmic decrement (log dec) δ, or its damping ratio ζ. Ginsberg [23] lists a well-known equation for the logarithmic decrement (δ) as derived from the ratio of two peak displacement amplitudes separated by N periods of motion,

$$\delta = \frac{1}{N}\ln\left(\frac{Z_k}{Z_{k+N}}\right) = \frac{2\pi\xi}{\sqrt{1-\xi^2}} = \xi\omega_n\tau_d \tag{3}$$

Eq. (3) is based on the transient free-response of an underdamped (ξ<1) one degree of freedom mechanical system, where

$$\zeta = \frac{C}{2\sqrt{K_S M}},\ \omega_n = \sqrt{\frac{K_S}{M}},\ \omega_d = \omega_n\sqrt{1-\xi^2},\ \tau_d = \frac{2\pi}{\omega_d} \tag{4}$$

Above, $M = M_{BC} + M_{SFD}$, where M_{BC}=15.15 kg and M_{SFD} is the SFD added mass, and K_S = 9.0 MN/m is the support structural stiffness where the system fundamental natural frequency $f_n = \omega_n/2\pi$ =124 Hz.

Figure 6 shows the displacement transient response exponentially decaying overlaid with the damping envelope ($e^{-\xi\omega_n t}$) and the DFT for each displacement Z_X. The data corresponds to unidirectional impact loads with $F_{MAX}/(LD)$=2.5 bar and 6.1 bar an initiating from the centered condition (e_s=0), and $F_{MAX}/(LD)$=5.4 bar for motions from static eccentricity (e_s/c=0.6). The BC transient response decays faster for the larger applied impact load and higher static eccentricity. Note that ten peaks (N=10) in the transient response are used to derive the logarithmic decrement (δ). The majority of the physical model fits ($e^{-\xi\omega_n t}$) show a high correlation factor (R^2>0.9) indicating the physical model is adequate to model the transient response of SFD subject to a single impact load. In the graphs, the DFT of a BC displacement is normalized with respect to the peak amplitude, $\overline{Z}_X(\omega) = Z_X(\omega)/Z_{MAX-X}(\omega)$, for a better comparison of all the obtained responses. Hence, in Fig. 6 (b), the maximum dimensionless displacement $\overline{Z}(\omega)$ equals one.

[1] Portions of this section reproduce ad-verbatim information presented in Ref. [21].

Figure 7 depicts the estimated SFD damping ratio (ζ) versus increasing peak BC dynamic displacement[2] (Z_{MAX}/c). The test data correspond to single impact load on SFD for motions from static eccentricity e_s/c=0.0c, 0.2c, 0.4c, and 0.6c. Note that the green dashed lines denote the BC static displacement $Z_{STAT} = (e_s/c)\cos(45^o)$. The damping ratio ($\zeta$) increases with both an increasing BC amplitude (Z_{MAX}) and the static eccentricity e_s.

[2] Z_{MAX} includes static displacement $Z_{STAT}=(e_s/c)\cos(45^o)$, see Eq. (1).

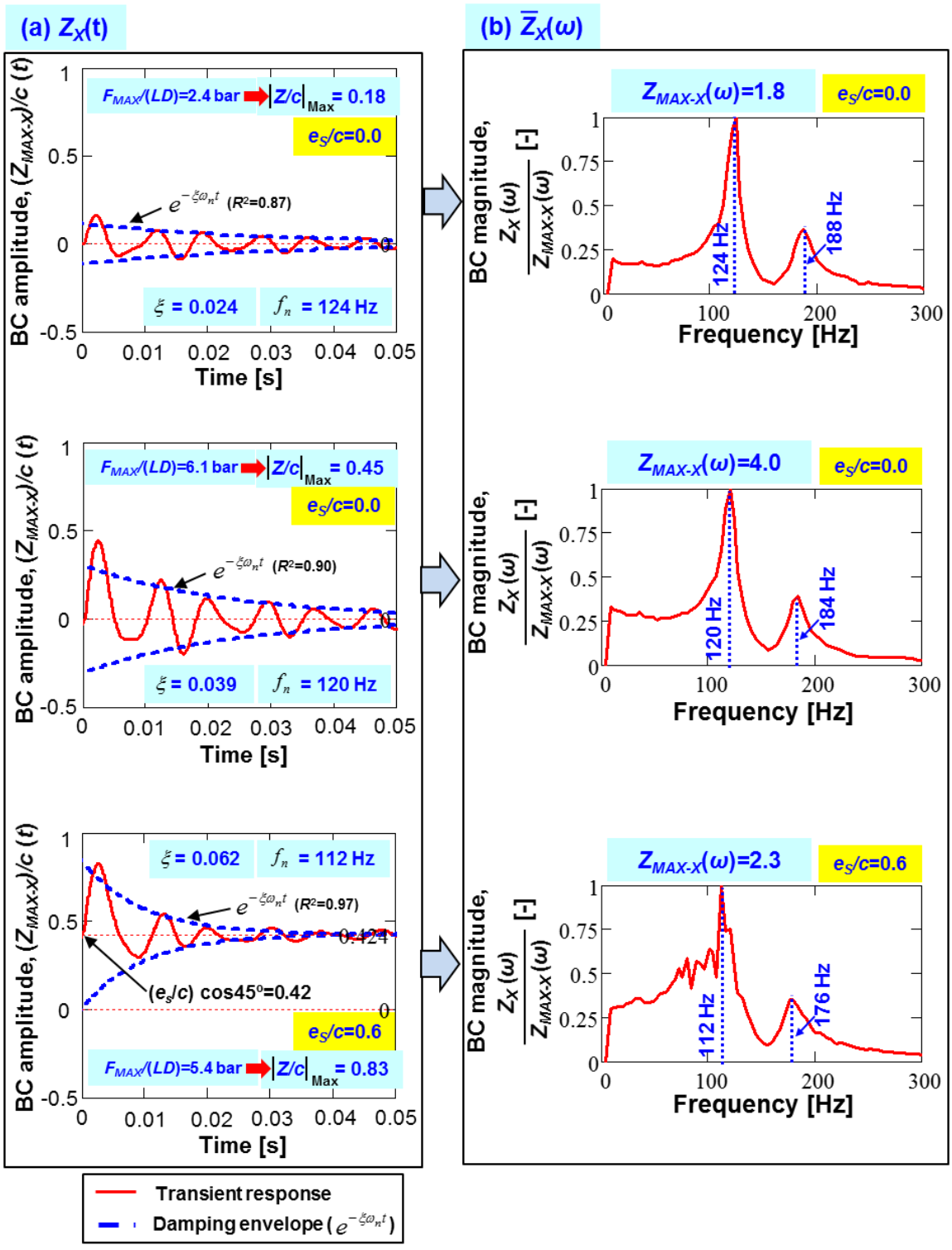

Figure 6. Peak BC dynamic amplitude Z_{MAX}/c and damping envelope ($e^{-\xi\omega_n t}$) versus time (t). Measurements for $F_{MAX}/(LD)$=2.5 bar & 6.1 bar for motions from e_s/c=0, and for $F_{MAX}/(LD)$=5.4 bar for displacements from e_s/c=0.6. Amplitude of DFT for Z_X also shown.

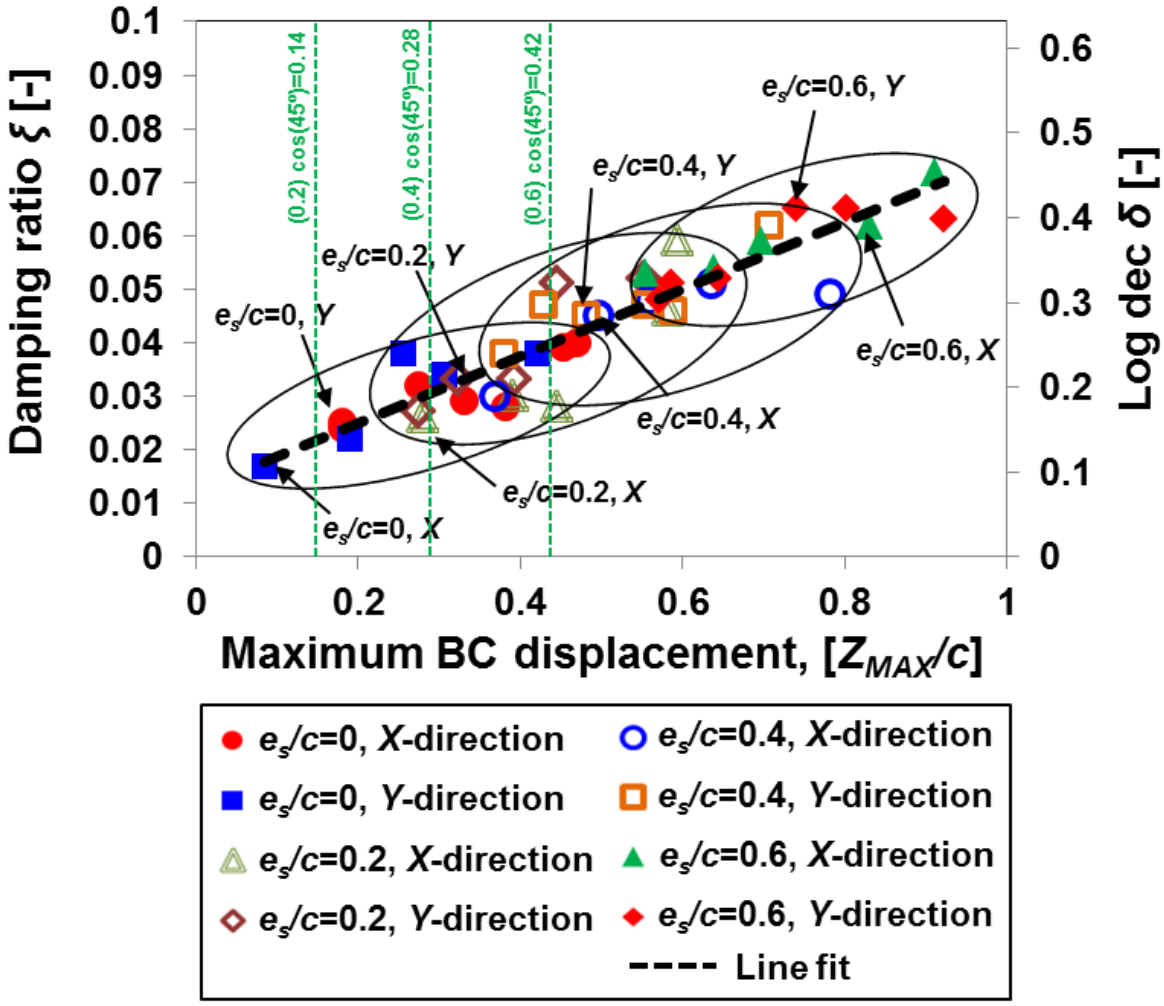

Figure 7. System damping ratio (ζ) and logarithmic decrement (δ) vs. peak displacement (Z_{MAX}/c). Data for one impact load and motions departing from various static eccentricity. Open-ends SFD with c=0.267 mm and 25.4 mm length film land.

Ref. [21] also reports measurements of system transient response due to a single impact load of increasing magnitude and motions starting at the centered position (e=0). In Ref. [21], however, the open ends test damper has a radial clearance of c_s=213 μm. Table 3 lists the distinct operating conditions for the two test SFDs with identical film land length L=25.4 mm and diameter, as well as lubricant inlet and temperature.

Table 3. Open ends SFD configurations and operating conditions for two film clearances

Parameter	Current c SFD	Small c_s SFD [21]
Radial clearance	267 μm	213 μm
Static groove pressure, P_G	0.34 bar(g)	0.37 bar(g)
Inlet flow rate, Q_{in}	5.0 LPM	4.5 LPM

Figure 8 shows comparisons of the damping ratio (ζ) estimated from both SFDs differing in clearance but with identical film land length. For small to moderate BC amplitude motions $Z_{MAX}/c<0.5$, the estimated SFD damping ratio for the small film clearance (c_s) [21] is ~1.3 to ~1.6 times larger than the damping ratio (ζ) obtained with a larger clearance (c). Classical lubrication theory predicts that for a short length open ends SFD, the damping (C) and inertia (M) coefficients are proportional to $1/c^3$ and $1/c$, respectively. Recall $\zeta \sim C/M$; hence, the damping ratio (ζ) scales approximately with the square of the film clearance, i.e., $\zeta \sim 1/c^2$. The small clearance damper generates ~1.3 to ~1.6 times more damping, the theoretical ratio of coefficients scales as

$$\frac{\xi_s}{\xi} \sim \left(\frac{c}{c_s}\right)^2 = \left(\frac{267}{213}\right)^2 = 1.57 \qquad (5)$$

Appendix D presents an analysis of the measured dynamic pressures in the film land. In brief, with a large static eccentricity $e_s/c=0.6$, the dynamic pressure at the minimum film thickness ($\Theta=225°$) is significantly higher than the pressure at other locations.

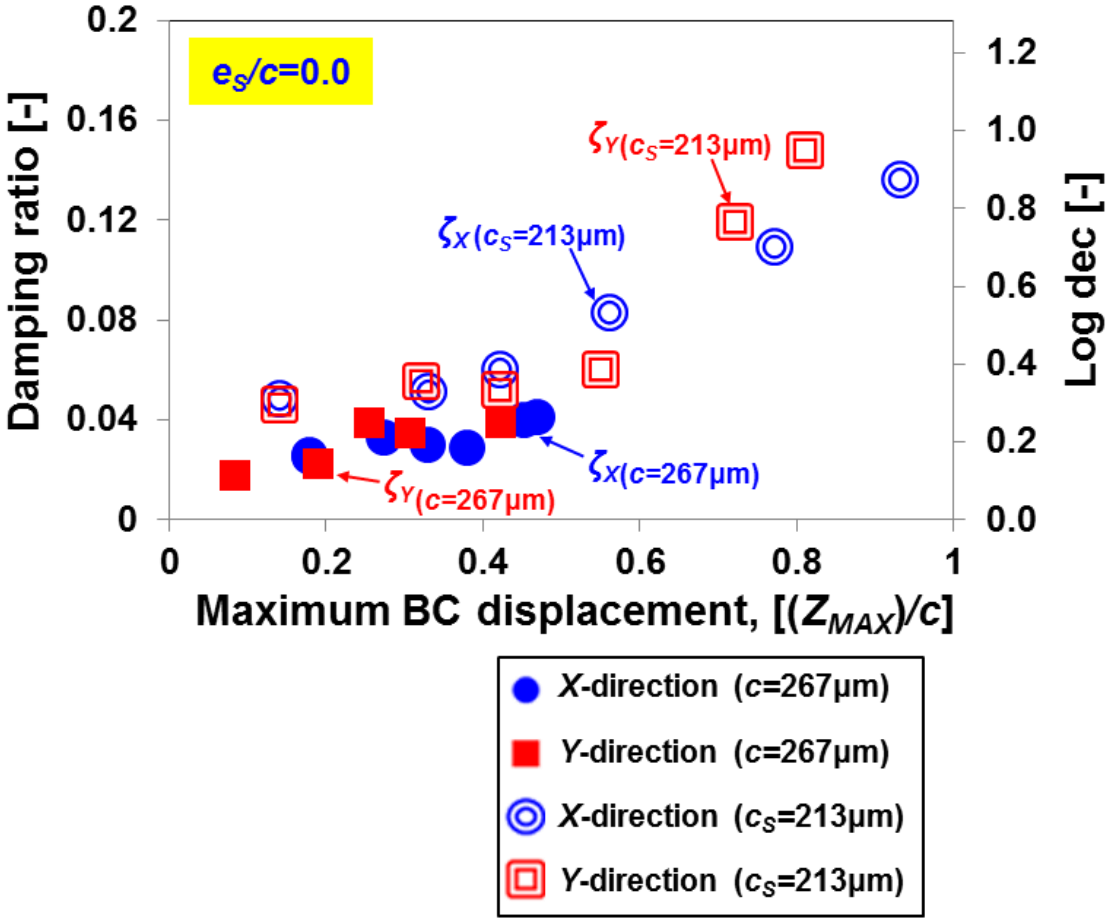

Figure 8. SFD damping ratio (ζ) versus peak BC (Z_{MAX}/c) displacement. Open-ends SFD with c=267 μm and c_s=213 μm [21]. L= 25.4 mm. Parameters identified for motions initiating at static eccentricity e_s/c=0.

Series of Consecutive Impact Load Tests

Consecutive Impacts with Equal Force Magnitude

This section describes the experimentally recorded BC transient response due to a series of consecutive impact loads: from two to six over a given time span (0.25 s), and with T_i as an elapsed time between consecutive impacts.

Table 4 lists the experimental conditions performed with load amplitude F_{MAX}=0.5 – 2.0 kN ($F_{MAX}/(LD)$=1.6 – 6.2 bar) for motions initiating from the centered condition (e_s=0.0c). Note that the time duration of each impulse load is ~1.4 ms and the average time interval between impacts is T_i =~30 ms, approximately ~3.7 times the natural period of the test rig $T_n=2\pi/\omega_{n1}$=8.2 ms.

Table 4 Operating conditions for test damper excited with repeated impact loads of equal magnitude. (Inlet flow rate Q_{in}=5 LPM, static inlet pressure P_{in}=0.34 bar(g), static eccentricity e_s=0).

Radial clearance c (μm)	Motion Type	Number of impacts	Duration of impact (ms)	Time between impacts (ms)	Average of # test sets	External load, F_{MAX} (N)	$F_{MAX}/(LD)$ (bar)
267	Series of consecutive impacts	2, 3, 4, 6	1.4	30	20	500	1.6
						750	2.3
						1000	3.1
						1500	4.7
						1750	5.4
						2000	6.2

Figure 9 depicts the typical time trace of (a) multiple impact loads, two to six, delivered to the BC and (b) the ensuing BC displacements (Z_X, Z_Y). The data is for $F_{MAX}/(LD)$=3.1 bar (F_{MAX}=1.0 kN) for motions from e_s/c=0, the centered condition. In Figure 9 (b), vertical blue dash lines indicate the time incidence of a peak external load. Expectedly, the maximum BC displacement occurs after the peak external load. Note that a second impact acts before the BC amplitude decays to rest. In the discussion below,

cases 2 thru 6 refer to the responses recorded from two to six consecutive impact loads, respectively.

Note that in some instances, an impact load shows a follow up load of lower or higher amplitude. These occurrences are random since a sequence of impacts (with a preset external force) applies to the BC as this may still be oscillating. During the transient response of the BC, the recorded following impact load depends on the location of the BC that is, either approaching the stinger or moving away from it.

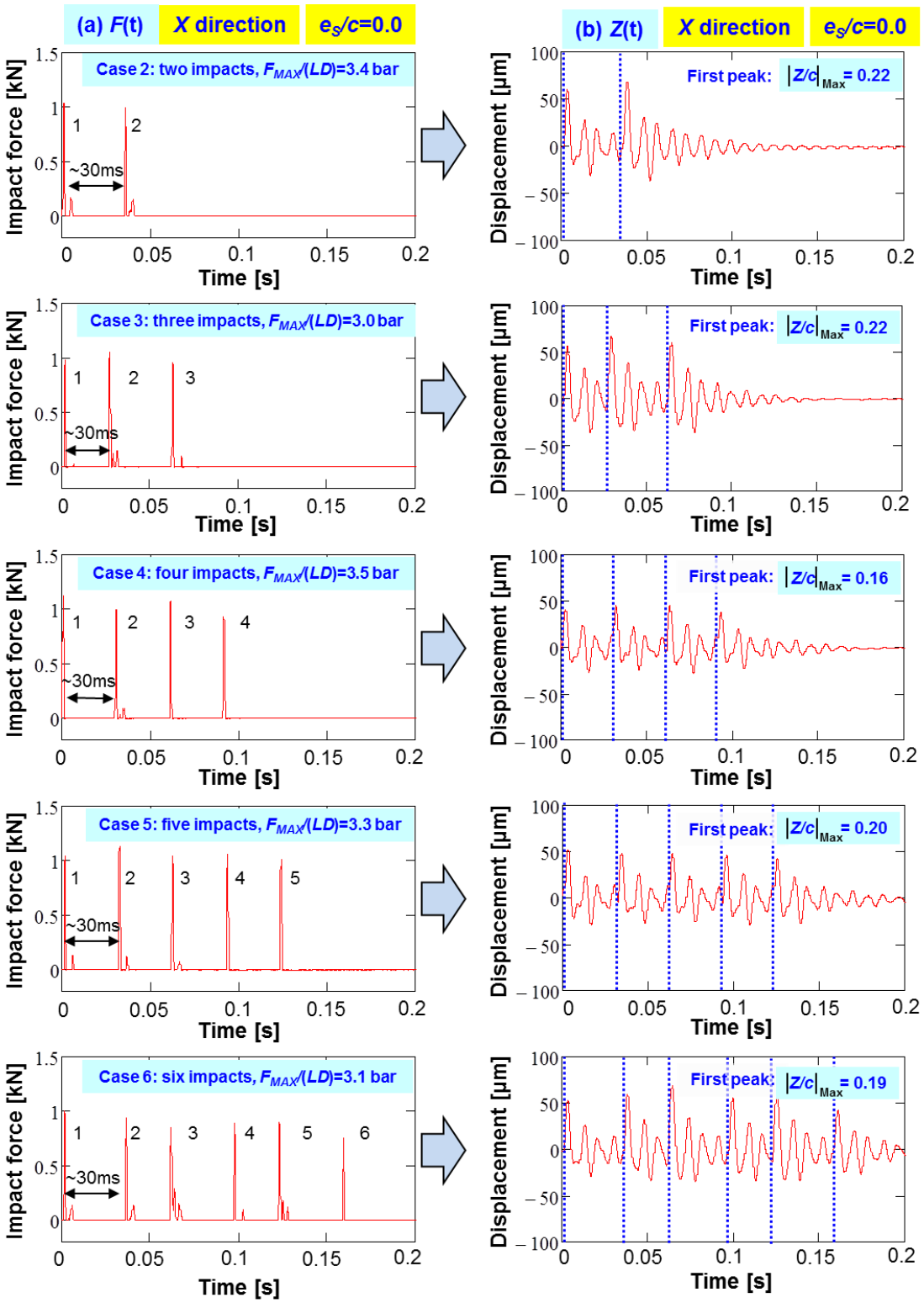

Figure 9. (a) Sets of repeated (2-6) impact loads *F*(t) and (b) ensuing BC displacement *Z*(t) vs. time. Measurements for $F_{MAX\text{-}X}/(LD)$~3.1 bar and motions initiating from static eccentricity e_S/c=0. Average elapsed time between impacts T_i =~30 ms.

Transient Response Characteristics

Figure 10 depicts the peak BC displacement ($|Z_{X,Y}|_{MAX}/c$) versus the peak amplitude of the impact ($F_{MAX}/(LD)$) for cases 2 and 3, i.e., two and three consecutive impact loads, respectively. **Appendix E** shows the rest of the maximum applied loads and ensuing maximum BC displacements $(|Z|_{MAX}/c)_{X,Y}$ for four, five, and six repeated impact loads. Insets on the top of each figure show the time trace of applied impact and the ensuing BC displacement. The straight line passing represents the simple curve fit of peak displacement over unit load, $(Z_{MAX}/c)/(F_{MAX}/(LD))$. The second peak BC amplitude is larger than the first, yet not necessarily larger than the third, for example.

Figure 11 shows the peak BC amplitude $(|Z|_{MAX}/c)_{X,Y}$ over unit load $(F_{MAX}/(LD))$ versus the number of impacts applied on the BC. Note that the test data corresponds to an elapsed time T_i=30 ms between impacts.

Z_{MAX}/F_{MAX} tends to increase with the number of applied consecutive impacts albeit **showing a large variability in the identification of results, perhaps due to the averaging procedure** (from 20 impacts).

Digression: To the Principal Investigator, the data is incongruent even though the test system is deterministic; hence largely unexplained. Irrespective of the number of impacts applied, since they are spaced apart by $T_i >> T_n$, the first peak amplitude should be identical for all cases: one, two, …, n impacts. Similarly, for series of two or more consecutive impacts, the second peak amplitude should be identical. For three or more impacts, the third peak of motion should have the same amplitude, and so forth. The data in Fig. 11 shows largely unexplained differences, as the test rig operator and research assistant do not mention the standard deviation (variability) for any of the tests reported.

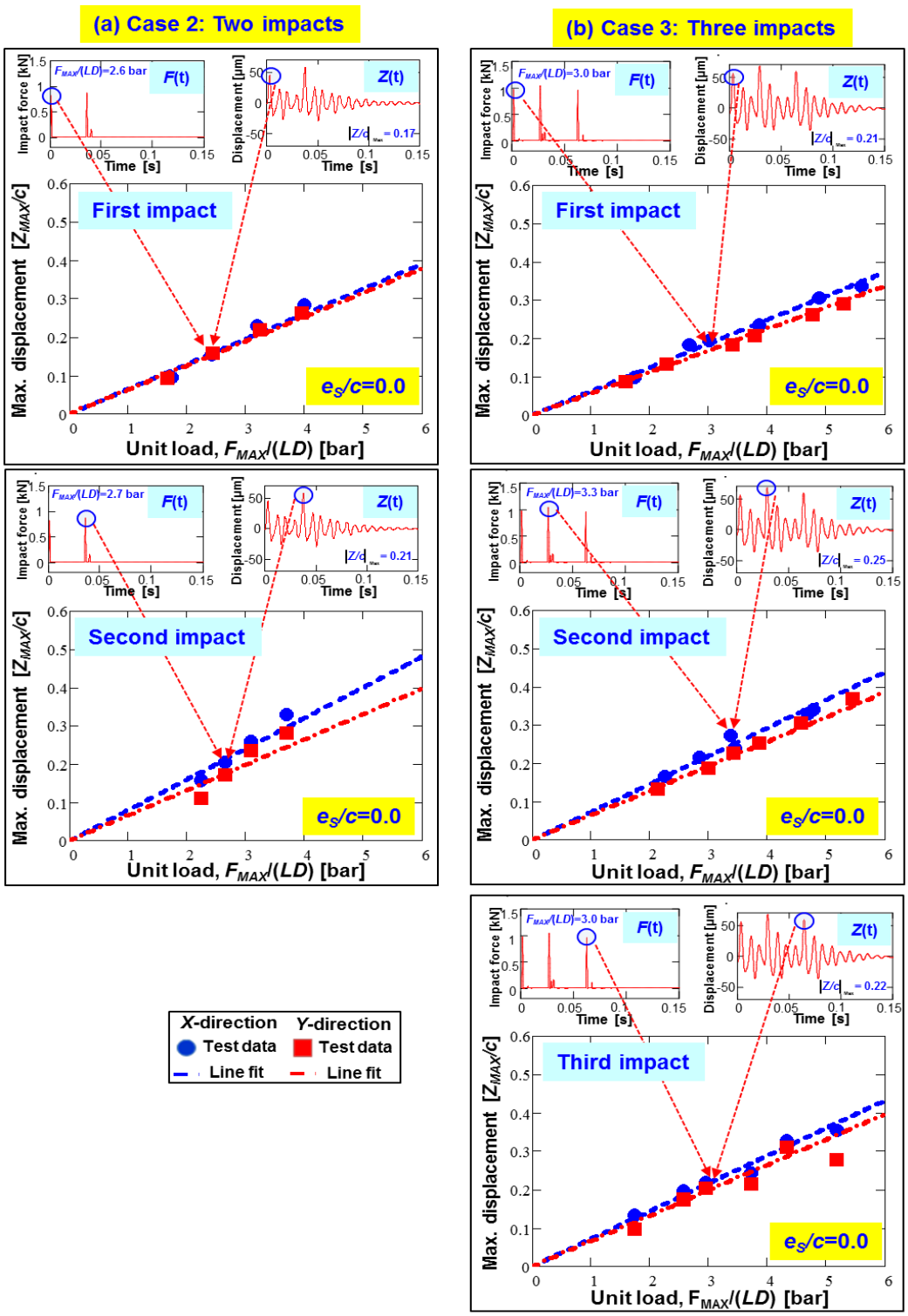

Figure 10. Maximum displacement $|Z_{MAX}|_{X,Y}/c$ vs. peak amplitude of unit load $F_{MAX}/(LD)$ for motions from centered condition (e_S/c=0.0). Data from two and three consecutive impacts with elapsed time between impacts T_i~30ms. Open ends SFD clearance c=0.267 mm (Insets show time traces of impact load and ensuing BC displacement).

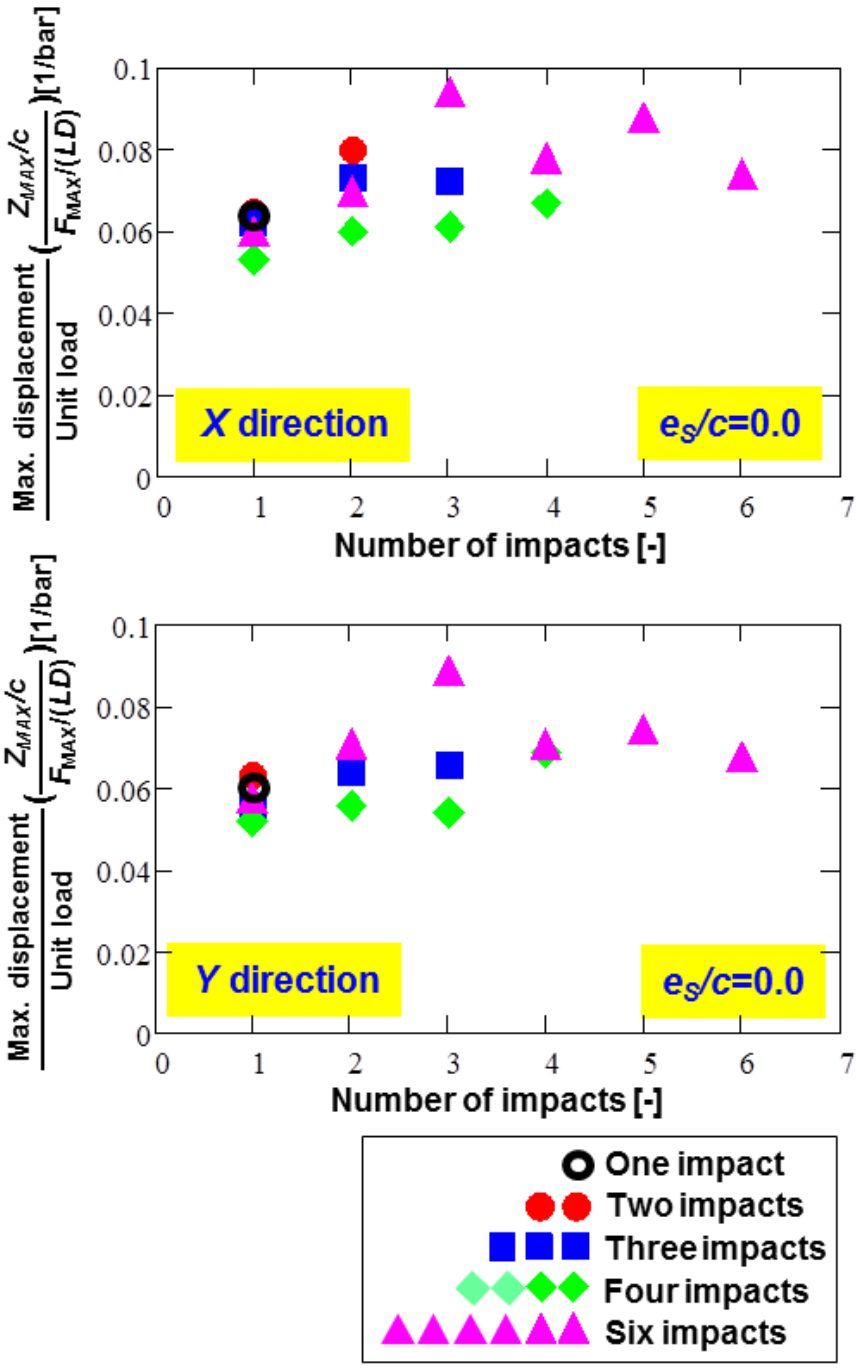

Figure 11. Peak displacement $|Z|_{MAX}/c$ over peak amplitude of unit load $F_{MAX}/(LD)$ vs. number of impacts for motions initiating from the centered condition (e_s/c=0.0). Tests with increasing number of impacts from one to six. Average elapsed time between impacts T_i =~30 ms. (Open ends SFD clearance c=0.267 mm).

Figure 12 depicts the BC velocity and displacement due to six consecutive impact loads (F_{MAX}=672 N) for motions from e_s/c=0. The elapsed time between impacts is T_i~30 ms. the figure presents a normalized displacement with respect to the peak amplitude $\overline{Z}_X(t) = Z_X(t)/Z_{MAX}(t)$, for example. Hence, the maximum dimensionless $\overline{Z}(t)$, $\overline{V}(t)$ and $\overline{F}(t)$ equal one. Note that the BC velocity is a discrete function constructed from the BC displacement, i.e., $V_i=(Z_{i+1}-Z_{i-1})/(2\Delta t)$. Figure 12 (a) shows (as it should) the peak BC displacement occurs when the BC velocity is zero, i.e., a phase lag of 90°. In Figure 12 (b), the BC velocity closely follows the time trace of the impact load and peaks just after the maximum force F_{MAX} is delivered.

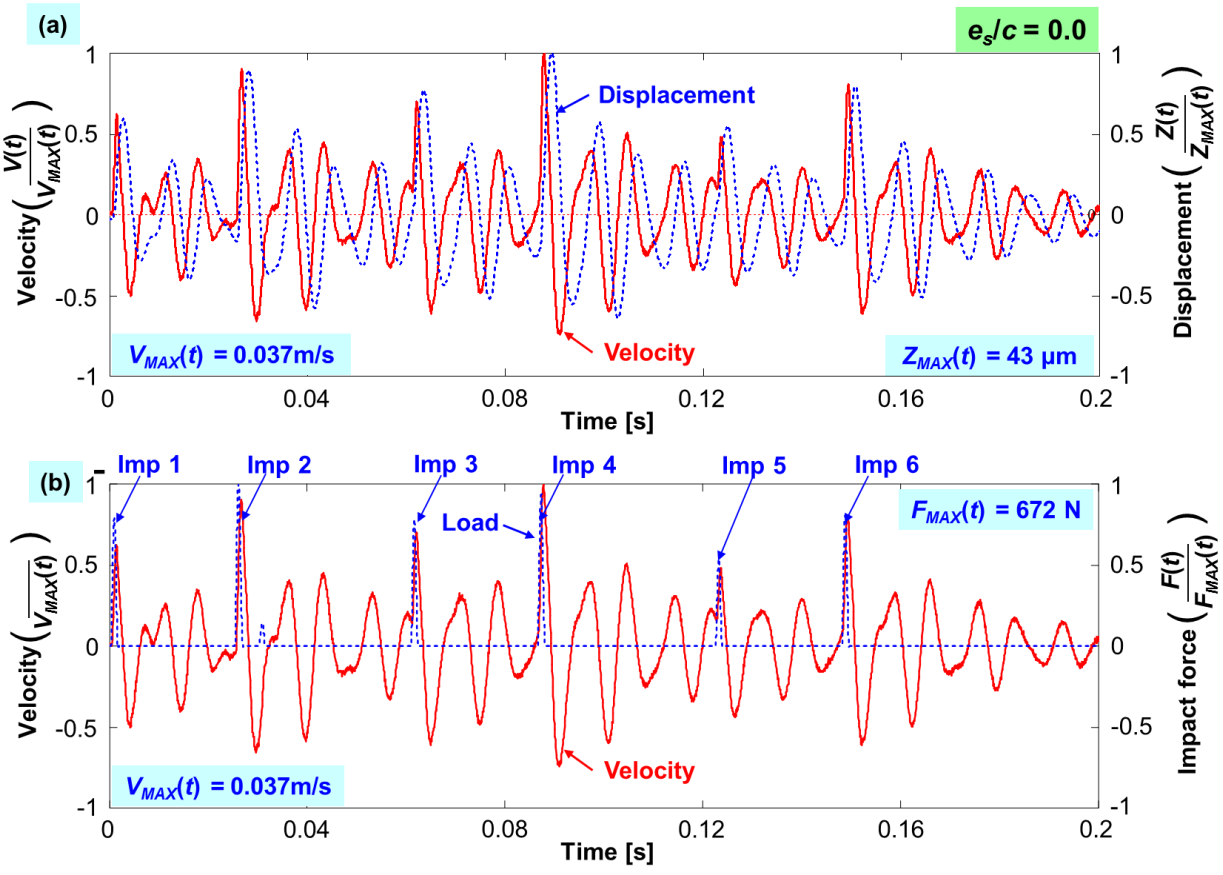

Figure 12. Normalized (a) BC displacement and velocity, and (b) velocity and impact loads vs. time for motions from e_s/c=0. Graphs shows data for six impacts (F_{MAX}=672 N). Elapsed time between impacts is T_i=~30 ms.

System Transient Response to a Series of Impacts of Varying Load Amplitude

An aircraft experiences a hard landing when the vehicle steeply descents to ground. During this event, a sudden upward force applies on the vehicle. In some cases, after touch down, subsequent smaller amplitude load impulse follow the initial upward force as the vehicle continues to roll on the runway.

Table 5 shows the operating conditions for a series of repeated impact tests with a decaying shock force amplitude. Note, the elapsed time between impacts is 0 s. That is, a second impact follows immediately the preceding one.

Table 5 Operating conditions for test damper with multiple impacts of decaying force amplitude. (Inlet flow rate Q_{in}=5 LPM, static inlet pressure P_{in}=0.34 bar(g)).

Radial clearance, c (μm)	Motion Type	Sets	Duration of impact (ms)	Time between impacts (ms)	Number of Consecutive impacts	External load, F (N)	$F/(LD)$ (bar)	Static eccentricity e_s/c (-)
267	Multiple unidirectional impacts	20	1.4	0	1, 3, 4	500	1.6	0, 0.2, 0.4, 0.6
						750	2.3	
						1000	3.1	
						1500	4.7	
						1750	5.4	
						2000	6.2	
						2250	7.0	
						2500	7.8	

Figure 13 shows three cases of impact load: (a) one single large amplitude impact, (b) a series of three consecutive impacts, and (c) a series of four consecutive impacts. In all cases, the motions begins at e_s/c=0, the centered condition. In the tests, the second impact is set to deliver a 50% load amplitude of the first one, while the third impact has 50% of the second one. In the graphs on the left, a vertical dash line denotes the true time incidence of the peak external load. The time lag between the occurrence of the peak external load and the maximum BC displacement is noticeable. Important enough, for case 4 (four consecutive impacts) with $F_{MAX}/(LD)$=7.9 bar, the time response of the BC does not oscillate about Z=0.

For the largest load $F_{MAX}/(LD)$=7.9 bar, see Figure 13(B) for case 4, the load sensor catches an additional impact force after the four consecutive impacts. This indicates that the BC touches the stinger before the stinger retracts back to its initial position. Note, at rest, stinger is 0.254 mm away from the BC.

Note the rebound of the BC after a large continuous impact is hard to avoid during the experiments since the transient response happens over a very short time. The (apparent) force recorded due to a rebound, after the three or four consecutive impacts, does not affect the magnitude of peak BC amplitude. At the moment of a rebound the BC displacement has already passed its peak amplitude.

DIGRESSION: To the Principal Investigator, the explanation is not plausible as during a rebound the BC pushes (back) into a stinger, and the recorded force should be negative. The test data reveals a flaw in the DAQ process constructing the impact loads.

Similar to Figure 12, Figure 14 depicts the BC velocity and displacement due to for four consecutive impact loads with $F_{MAX}/(LD)$=3.0 bar (F_{MAX}=992 N) and $F_{MAX}/(LD)$=7.9 bar (F_{MAX}=2,540 N) for motions departing from e_s/c=0. Recall the elapsed time between impacts is T_i=0 ms. The test data shown in the figure is normalized with respect to the respective peak amplitude, thus the maximum dimensionless $\overline{Z}(t)$, $\overline{V}(t)$ and $\overline{F}(t)$ equal one. In Figure 14, the BC velocity tends to decrease gradually (not as fast as the data in Figure 12) due to the immediacy of the consecutive impact load. At the incidence of an impact (circled in black), the external force acts as an impulse adding (positive) BC velocity to the system. That is,

$$V_{new} = V_{t=imp} + \frac{\int_0^{1.4ms} F\,dt}{M_{BC}} \tag{6}$$

where $V_{t=imp}$ is the BC velocity just before the impact is applied.

Figure 15 depicts the maximum applied unit load $F_{MAX}/(LD)$ and ensuing maximum BC displacements (Z) from motions departing from static eccentricity e_s/c=0.0, 0.2, 0.4, and 0.6 for (a) a single impact, (b) a series of three consecutive impacts and (c) a series of four consecutive impacts. Each data point represents the average of 20 maximum $(Z\ \&\ F)_{MAX}$. The line passing through the data points represents the line fit of peak displacement over unit load, $(Z/c)/(F/(LD))_{MAX}$ for each static eccentricity. Note that the static eccentricity (e_s) is 45° away from the X and Y axes. As expected, the BC amplitude

increases with the increase in number of applied impacts, as they add (kinetic) energy into the test system, see Figure 14 (a), for example.

Figure 16 shows the peak BC amplitude $(|Z|_{MAX}/c)_{X,Y}$ over unit load, $F_{MAX}/(LD)_{X,Y}$, versus static eccentricity (e_s/c). Z_{MAX}/F_{MAX} represents the magnitude of the line fit (slope) shown in Figure 15. The data correspond to results from a single impact load, three, and four consecutive impacts. The elapsed time between impacts is $T_i = 0$ ms. The magnitude of the peak displacement grows as the number of impacts increases and as the static eccentricity increases.

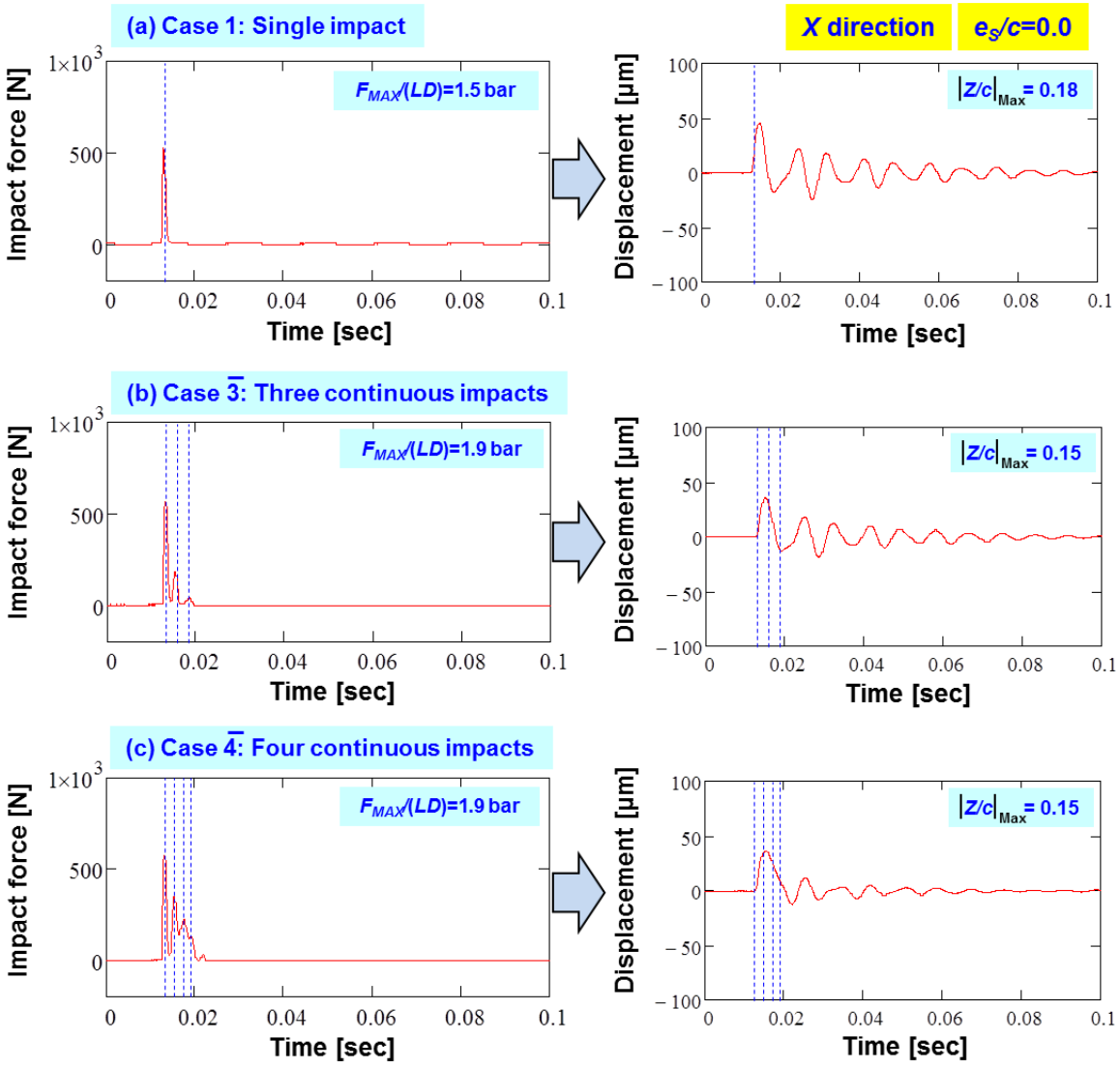

Figure 13 (A). Impact load *F*(t) and ensuing BC displacement *Z*(t) versus time for (a) Case 1: single impact, (b) Case 3: three consecutive impacts, and (c) Case 4: four consecutive impacts. Measurements for $F_{MAX}/(LD)$=1.9 bar and motions departing from static eccentricity e_s/c=0.

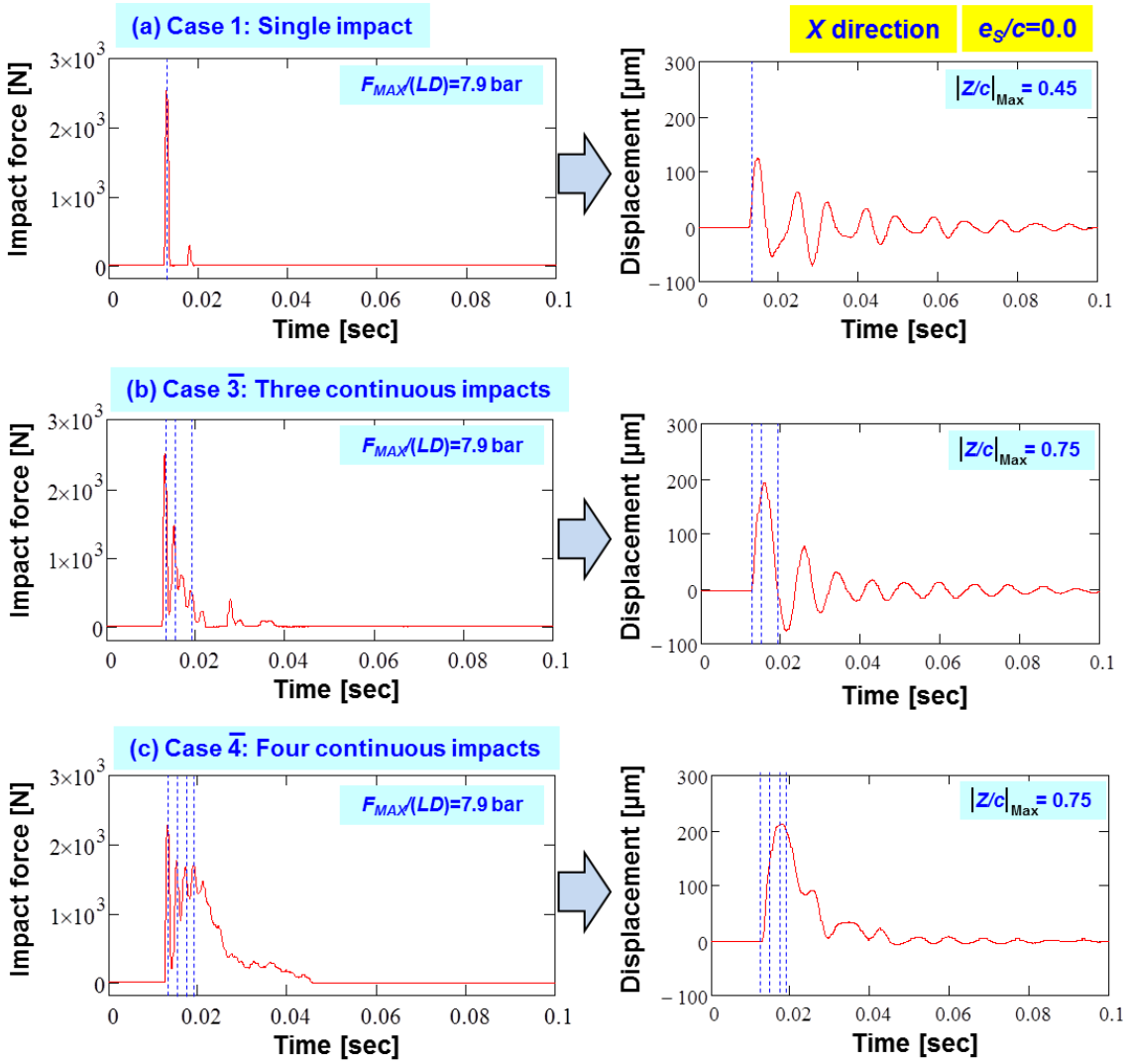

Figure 13(B). Impact load *F*(t) and ensuing BC displacement *Z*(t) versus time for (a) Case 1: single impact, (b) Case 3: three consecutive impacts, and (c) Case 4:four consecutive impacts. Measurements for $F_{MAX}/(LD)$=7.9 bar and motions departing from static eccentricity e_s/c=0.

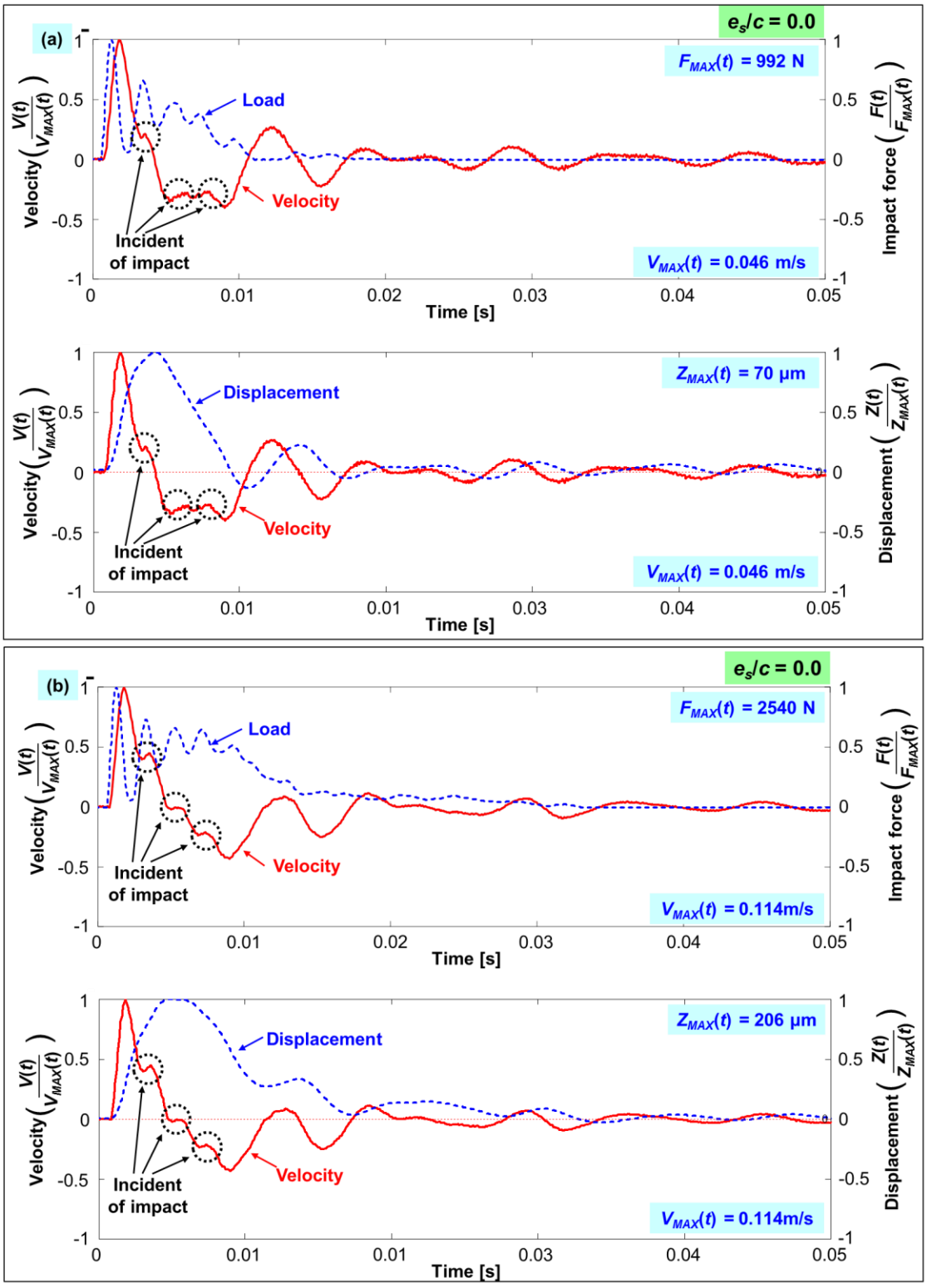

Figure 14. Normalized velocity and impact load and BC displacement and velocity vs. time for motions from e_s/c=0. Graphs shows data for four consecutive impacts for (a) F_{MAX}=992 N and (b) F_{MAX}=2,540 N. Elapsed time between impacts is T_i=~0 ms.

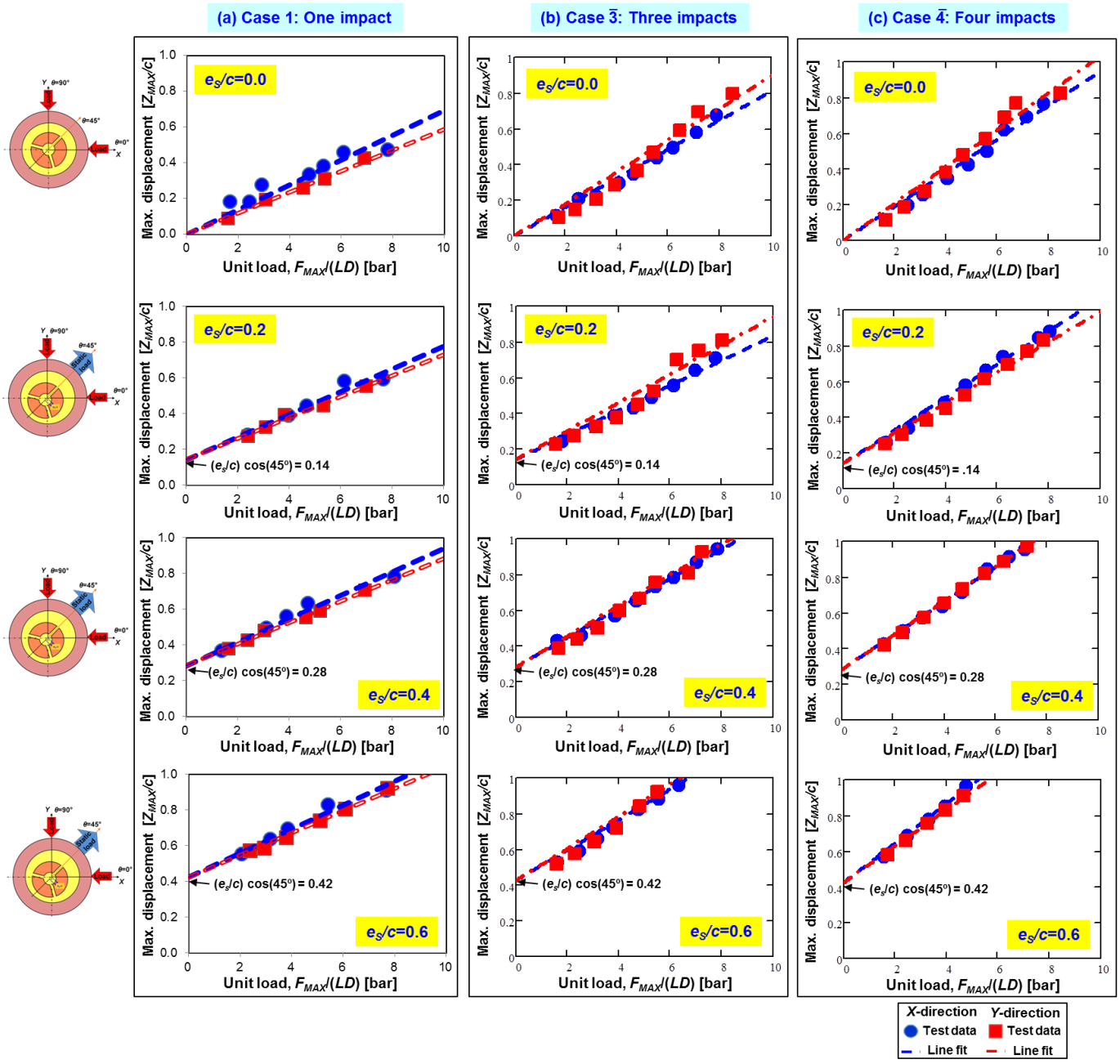

Figure 15. Ensuing maximum BC displacement $|Z_{MAX}|_{X,Y}/c$ versus peak unit load $F_{MAX}/(LD)$ for BC motions initiating from e_S/c=0.0, 0.2, 0.4, and 0.6. Tests with one, three and four consecutive impacts; elapsed time between impacts T_i=0 ms. (Open ends SFD nominal clearance c=267 μm.)

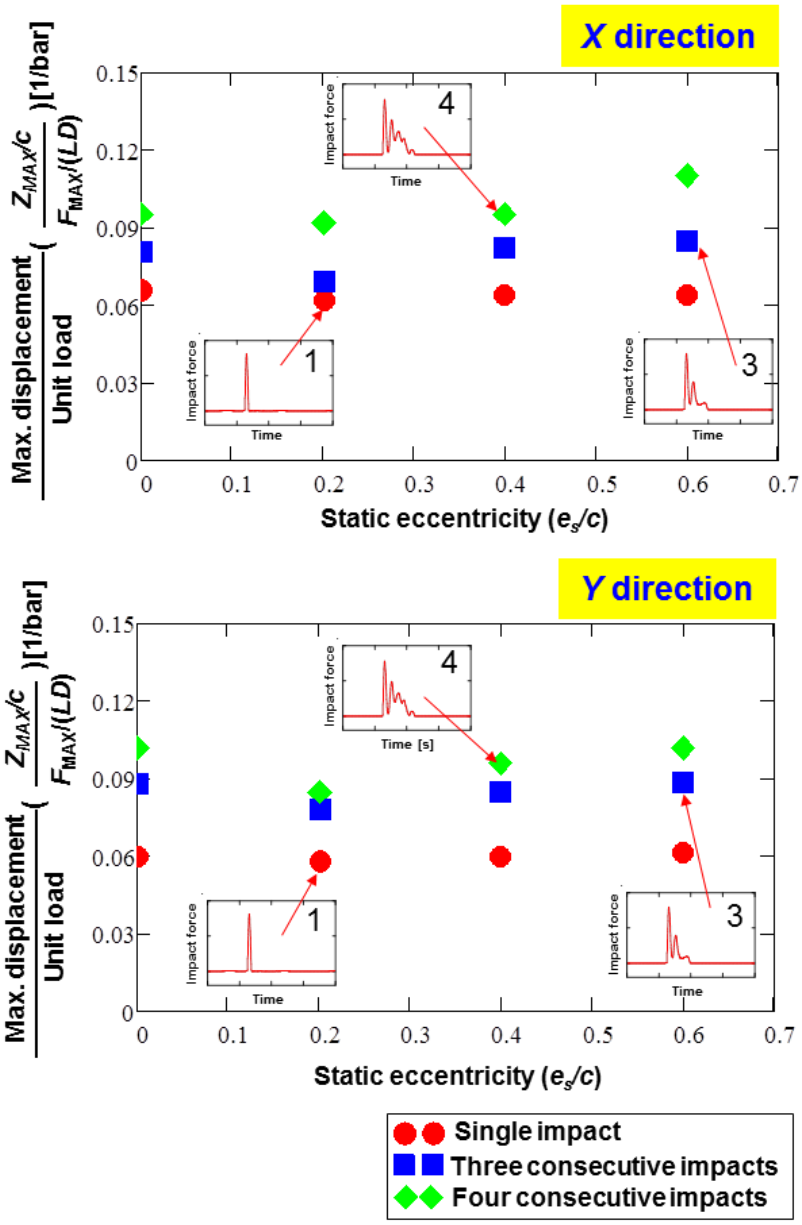

Figure 16. Peak displacement $|Z_{X,Y}|_{MAX}/c$ over peak amplitude of unit load $F_{MAX}I(LD)$ vs. static eccentricity (e_s/c). Tests with three and four consecutive impacts; elapsed time between impacts T_i=0 ms. Open ends SFD clearance c=0.267 mm.

Prediction of Transient Response for the Test System

This section provides a comparison between the experimental results and predictions of the transient response obtained with a computational program [24] that models a point mass rotor supported on short-length, open ends SFD. The model assumes a full film or 2π film (without oil cavitation)[3]. The simple model ignores the feed holes and their distribution around the bearing circumference.

In an open ends SFD, Ref. [2] states the following formulas for the axially averaged pressure field P,

$$P = P_V + P_I \tag{7}$$

that adds the viscous and inertial contributions given by

$$P_V = -\frac{\mu L^2}{h^3}(V_X \cos\theta + V_Y \sin\theta) \tag{8}$$

$$P_I = -\frac{\rho L^2}{12h}\left[a_X \cos\theta + a_X \cos\theta - \frac{2.4}{h}(V_X \cos\theta + V_Y \sin\theta)\right] \tag{9}$$

where the film thickness is $h = c + Z_X \cos\theta + Z_Y \sin\theta$. Above, ($Z_X$,$Z_Y$), ($V_X$,$V_Y$), and ($a_X$,$a_Y$) are the journal center displacement, velocity and acceleration, respectively.

The equation of motion for the point mass system is

$$M_{BC}\begin{pmatrix} a_X \\ a_Y \end{pmatrix} + \begin{pmatrix} C_{SX} & 0 \\ 0 & C_{SY} \end{pmatrix}\begin{pmatrix} \dot{z}_X \\ \dot{z}_Y \end{pmatrix} + \begin{pmatrix} K_{SX} & 0 \\ 0 & K_{SY} \end{pmatrix}\begin{pmatrix} z_X \\ z_Y \end{pmatrix} = \begin{pmatrix} F_{X(t)} \\ F_{Y(t)} \end{pmatrix} + \begin{pmatrix} F_{SFD-X} \\ F_{SFD-Y} \end{pmatrix} + \begin{pmatrix} F_{S_X} \\ F_{S_Y} \end{pmatrix} \tag{10}$$

where $\boldsymbol{F_S} = \begin{bmatrix} F_{S_X} & F_{S_Y} \end{bmatrix}^T$ is a static load, $\boldsymbol{F} = \begin{bmatrix} F_{X(t)} & F_{Y(t)} \end{bmatrix}^T$ is a dynamic load. K_S and C_S denote the structure stiffness and remnant damping. $\boldsymbol{F_{SFD}}$ is a function of the journal instantaneous displacement, velocity, and acceleration, i.e.,

$$\boldsymbol{F_{SFD}} = f(z_X, z_Y, \dot{z}_X, \dot{z}_Y, \ddot{z}_X = a_X, \ddot{z}_Y = a_Y) \tag{11}$$

and obtained from integration of the pressure fluid over the journal surface, i.e.,

$$F_{SFD-X} = RL\int_0^{2\pi} P_{(\theta)} \cos\theta \, d\theta \; ; \; F_{SFD-Y} = RL\int_0^{2\pi} P_{(\theta)} \sin\theta \, d\theta \tag{12}$$

Table 6 presents the physical parameters and the operating conditions to obtain predictions of the test system (mass, structure and SFD) transient response characteristics.

[3] The analysis ignores the sub ambient pressures recorded during the measurements, see Appendix D..

Table 6. Physical parameters for prediction of forces for short-length open ends SFD.

Parameter	Magnitude
Journal diameter (D)	126.7 mm
Nominal radial clearance (c)	267 μm
Film land length (L)	25.4 mm
BC mass (M_{BC})	15.15 kg
Ambient pressure, P_{amb}	0 bar(g)
Oil cavitation pressure, P_{cav}	-1 bar(g)
Oil viscosity (μ)	2.6 cPoise
Oil density (ρ)	800 kg/m^3
External load	500 – 2,500 N $F_{MAX}/(LD)$=1.6 - 7.8 bar
Structural stiffness, $K_{S\text{-}X,Y}$	9 MN/m
Structural damping, $C_{S\text{-}X,Y}$	0.1 kN.s/m
Duration of impact, T_{IMP}	1.4 ms
Elapsed time between impacts, T_i	30 ms

Predicted Transient Response Characteristics

Figure 17 shows the experimental and predicted peak BC (journal) amplitude ($|Z_{X,Y}|_{MAX}/c$) over unit load ($F_{MAX}/(LD)$) versus number of repeated impacts applied on the BC. Note that the time of each impulse is T_{IMP}=1.4 ms and the elapsed time between impact is T_i ~30 ms. Predictions for 2π film models show that ($|Z_{X,Y}|_{MAX}/c$)/($F_{MAX}/(LD)$) increases as the number of impacts increases to three, and then shows a relatively constant magnitude for more impacts. Compared to the measured responses, the model using the 2π film SFD model predicts the system response with moderate agreement. The discrepancy is most likely due to the simple model ignoring the feed holes and their distribution around the bearing circumference. **Appendix F** shows predicted transient response characteristics of peak BC displacement ($|Z_{X,Y}|_{MAX}/c$).

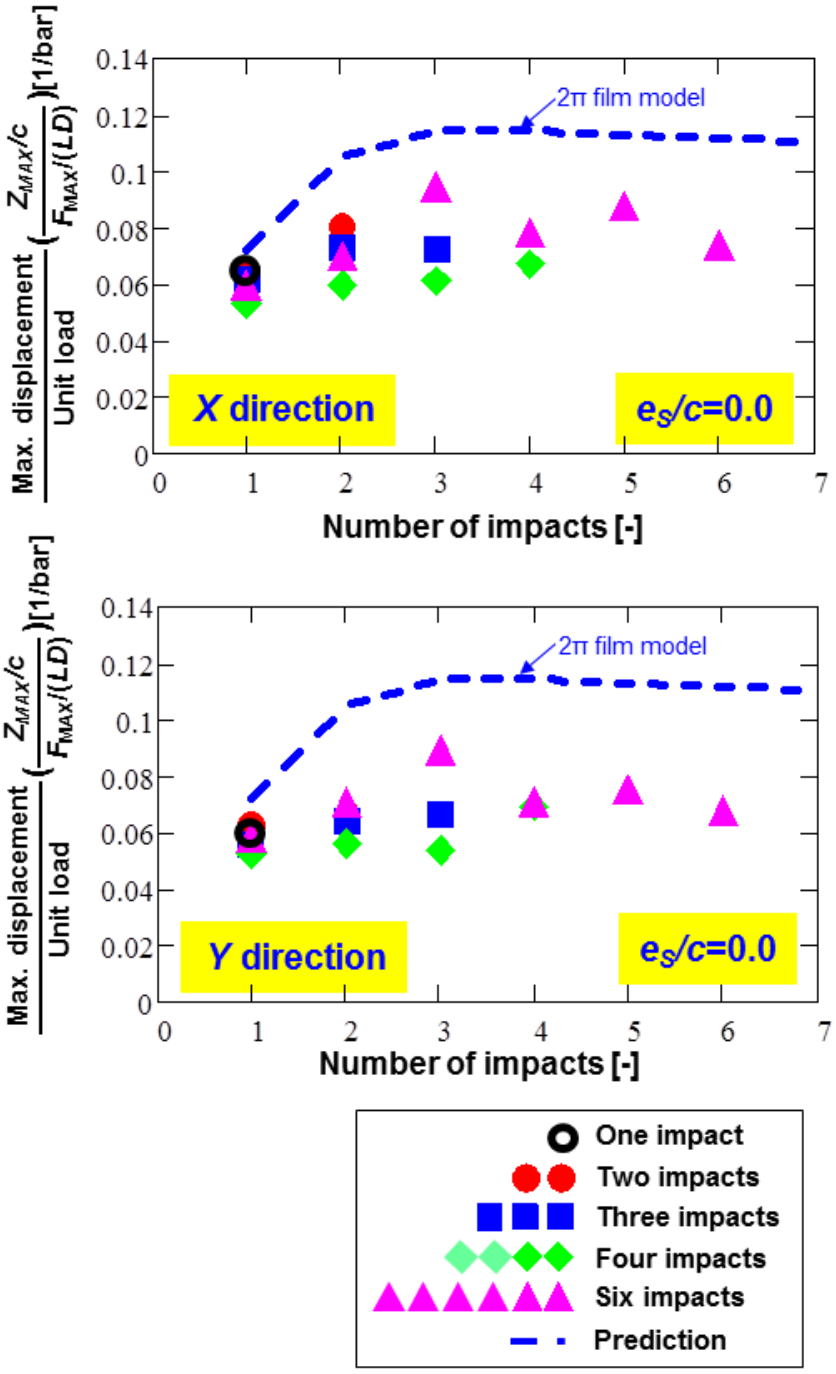

Figure 17 Comparison of experimental and predicted BC peak displacements $|Z_{X,Y}|_{MAX}/c$ over peak amplitude of unit load $F_{MAX}/(LD)$ vs. number of consecutive impacts for motions from e_s/c=0. Duration of impact T_{IMP}=1.4 ms and time between impacts T_i=30 ms. (Open ends SFD clearance c=0.267 mm.)

Conclusions and Recommendations

Tests with single and (repeated) consecutive impact loads were performed on a single land, open ends (L=25.4 mm) SFD. The peak amplitude of the impact load ranges from 0.5 – 2.5 kN and the motions begin from centered and off-centered conditions (max. 60% of clearance). The report provides a comprehensive analysis of the recorded peak amplitudes of motion derived from single impact loads, repeated and elapsed impacts with equal load magnitude, and consecutive and immediate impact loads with a decaying load amplitude. The major findings derived from the measurements are:

Analysis of Transient Response Characteristics,

(a) SFD BC transient response decays faster with a large amplitude applied impact load and departing from a high static eccentricity.

(b) For series of consecutive impacts, each T_i=30ms apart, a lesser unit load $F_{MAX}/(LD)$ is required for successive impacts to increase the peak BC amplitude.

(c) For a series of consecutive impacts, without time delay. with load amplitude at a fractional decay (T_i=0ms), the external force acts as an impulse adding kinetic energy to the system, and thus the BC peak amplitude increases with an increase in the number of consecutively applied impacts.

Damping ratio,

(a) The damping ratio (ζ) from single impact load is sensitive to both the external load F_{MAX} and the static eccentricity (e_s).

(b) Damping ratio for the small film clearance (c_s=0.213 mm) [21] is ~1.3 to ~1.6 times larger than the damping ratio (ζ) obtained with the current larger clearance damper (c=1.25 c_s). The damping ratio (ζ) scales approximately with the square of the film clearance, i.e., $\zeta \sim 1/c^2$.

Film land dynamic pressures,

(a) An increase in applied peak load F_{MAX} increases the *peak* dynamic film pressures.

(b) For motions departing from a large static eccentricity, the mid plane film dynamic pressure at the minimum film thickness location is an order of magnitude larger than the film pressure measured at other locations.

Further tests with end sealed SFD configuration to amplify the available damping with less lubricant flowrate are planned.

Acknowledgement

The financial support the Turbomachinery Research Consortium (TRC) is gratefully acknowledged. Special thanks to graduate student Mr. Sean Den for reviewing the initial draft of the report.

References

[1] Zeidan, F., San Andrés, L., and Vance, J. M., 1996, "Design and Application of Squeeze Film Dampers in Rotating Machinery," Proceedings of the 25th Turbomachinery Symposium, Turbomachinery Laboratory, Texas A&M University, Houston, TX, Sept. 16–19, pp. 169–188.

[2] San Andrés, L., 2012, *Modern Lubrication Theory*, "Squeeze Film Dampers: Operation, Models and Technical Issues," Notes 13, Texas A&M University Digital Libraries, http://repository.tamu.edu/handle/1969.1/93197

[3] San Andrés, L., 2012, "Damping and Inertia Coefficients for Two Open Ends Squeeze Film Dampers with a Central Groove: Measurements and Predictions," ASME J. Eng. Gas Turbines Power, **134**(10), p. 102506.

[4] San Andrés, L., and Seshagiri, S., 2013, "Damping and Inertia Coefficients for Two End Sealed Squeeze Film Dampers with a Central Groove: Measurements and Predictions," ASME J. Eng. Gas Turbines Power, **135**(12), p. 112503.

[5] San Andrés, L., and Jeung, S.-H., 2015, "Experimental Performance of an Open Ends, Centrally Grooved, Squeeze Film Damper Operating with Large Amplitude Orbital Motions," ASME J. Eng. Gas Turbines Power, **137**(3), p.032508.

[6] Barrett, L. E., and Gunter, E. J., 1975, "Steady-State and Transient Analysis of a Squeeze Film Damper Bearing for Rotor Stability," NASA CR-2548, Washington, D.C.

[7] Gunter, E. J., Barrett, L. E., and Allaire, P. E., 1977, ''Design of Nonlinear Squeeze Film Dampers for Aircraft Engines,'' ASME J. Lubr. Technol., 99, No. 1, pp. 57–64.

[8] Stallone, M.J., Gallardo, V., Storace, A.F., Bach, L.J. and Black, G., 1983, "Blade Loss for Transient Dynamic Analysis of Turbomachinery", AIAA J. **21**(8), pp. 1134–1138.

[9] Sun, G., Kaushik, N., Palazzolo, A., Provenza, A., Lawrence, C., Carney, K., 2003, "An Efficient Algorithm for Blade Loss Simulations using a High Fidelity Ball

Bearing and Damper Model," Proc. ASME 19th Biennial Conference on Mech. Vib. and Noise, Chicago, USA, DETC 2003/VIB 48424.
[10] Sun, G., Palazzolo, A., Provenza, A., Lawrence, C., and Carney, K., 2008, "Long Duration Blade Loss Simulations Including Thermal Growths for Dual-Rotor Gas Turbine Engine," J. Sound Vib., **316**, pp. 147–163.
[11] Zhang, S. P., Yan, L. T., and Li, Q. H., 1991, "Development of Porous Squeeze Film Damper Bearings for Improving the Blade Loss Dynamics of Rotor-Support Systems," ASME J. Vib., Acoust., **114**, pp. 347–353.
[12] Zhang, S. P., Yan, L. T., and Li, Q. H., 1993, "The Effectiveness of Porous Squeeze Film Dampers for Suppressing Nonsynchronous Motions," ASME J. Vib., Acoust., **115**, pp. 16–18.
[13] Walton, J. F., and Heshmat, H., 1993, "Rotordynamic Evaluation of an Advanced Multi-squeeze Film Damper-Imbalance Response and Blade-Loss Simulation," ASME J. Engineering for Gas Turbines and Power, **115**, pp. 347-352,
[14] Ishii, T., and Kirk, R. G., 1996, "Transient Response Technique Applied to Active Magnetic Bearing Machinery During Rotor Drop," ASME J. Vibr. Acoust., 118, pp. 154–163.
[15] Sun, G., and Palazzolo, A., 2006, "Rotor Drop and Following Thermal Growth Simulation Using Detailed Auxiliary Bearing and Damper Models," J. Sound Vib., **289**, pp.334–359.
[16] Sun, G., 2006, "Auxiliary Bearing Life Prediction Using Hertzian Contact Bearing Model," ASME J. Vib., Acoust., 128, pp. 203–209.
[17] Roberts, J. B., Holmes, R., and Mason, P. J., "Estimation of Squeeze-Film Damping and Inertial Coefficients from Experimental Free-Decay Data," *Proceedings of the Institution of Mechanical Engineers,* Engineering Sciences Division, Vol. 200, No. 2C, 1986, pp. 123-133.
[18] Ramli, M. D., Roberts, J. B., and Ellis, J., 1987, "Determination of Squeeze Film Dynamic Coefficients from Experimental Transient Data," ASME J. Tribol., **109**, pp. 155–163.
[19] Roberts, J. B., Ellis, J., and Hosseini Sianaki, A., 1990, "The Determination of Squeeze Film Dynamic Coefficients from Transient Two-Dimensional Experimental Data," ASME J. Tribol., **112**, pp. 288–298.
[20] Lee, A., Kim, B., and Kim, Y., 2006, "A Finite Element Transient Response Analysis Method of a Rotor-Bearing System to Base Shock Excitations Using the State-Space Newmark Scheme and Comparisons With Experiments," J. Sound Vib., **297**(3–5), pp. 595–615.
[21] San Andrés, L., Jeung, S.-H., and Ghaznavi, Z., 2014, "Response of an Open Ends Squeeze Film Damper to Large Amplitude Impact Loads," TRC-SFD-01-2014, Turbomachinery Research Consortium Technical Report, Texas A&M University, College Station, TX, USA.
[22] San Andrés, L., and Jeung, S.-H., 2015, "Response of an Open Ends Squeeze Film Damper to Large Amplitude Impact Loads," *Proceedings of the 2015 STLE Annual Meeting (Extended Abstract)*, Dallas, TX.
[23] Ginsberg, J. H., 2001, *Mechanical and Structural Vibration – Theory and Application*, John Wiley & Sons, New York, pp. 79–85.

[24] San Andrés, L., 2014, “Transient Response of a Point Mass Supported on Short Length Squeeze Film Dampers Including Fluid Inertia Effect,” Personal Communication.

Appendix A. Identification of (Dry) Test System Structure Parameters

Four main rods support the current bearing cartridge (BC). Figure A.1(a) displays a schematic view of the static load test setup. One eddy current REBAM® displacement sensor, mounted externally to a magnetic base, aligns with the *X*, *Y*, or 45° directions. This sensor is referred as an external sensor and has a known sensitivity. By measuring the force from the static loader, data from the external sensor serves to measure the structural stiffness of the supports.

Figure A.1 (b) shows BC displacement versus the static load applied for each orientation of the external sensor. The estimated structural stiffness is K_S=9.2 MN/m for a BC displacement the direction of applied load. The stiffnesses are K_{SX}=8.8 MN/m and K_{SY}=9.3 MN/m along the *X* and *Y* axes, respectively. Note that the structural stiffness along the *X* axis is ~5% lower than the that along the *Y* axis.

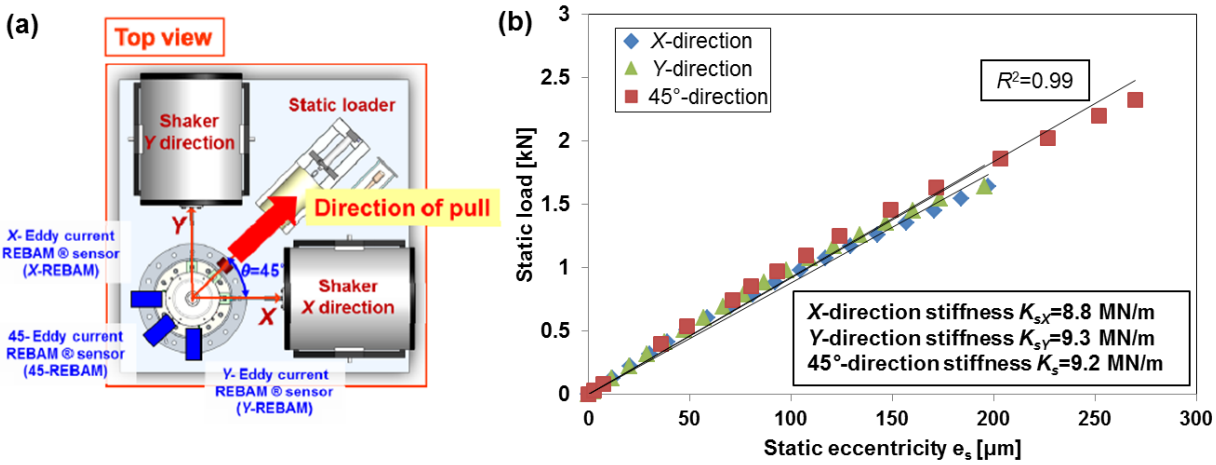

Figure A.1. (a) Schematic view of static load test setup and (b) static load versus BC displacement and estimated structural stiffness along the *X*, *Y* axes and along the 45° direction.

An impact is delivered to the bearing cartridge assembly along the *X* direction, *Y* direction and 45° away. Note that no lubricant in the SFD land during the impact test and thus the natural frequency obtained corresponds to the dry-structure. The accelerometer measure the acceleration of the bearing cartridge resulting from the applied impact.

Figure A.2 shows the transient time response of the bearing acceleration for the external loads and its DFT (discrete Fourier transform) along the *X*, *Y* directions and 45^o away. In the graphs, the BC acceleration is normalized with respect to the peak amplitude, $\bar{a}_X(\omega) = a_X(\omega)/a_{MAX-X}(\omega)$, for a better comparison of all the obtained responses. The response of the system is characterized by an oscillatory response with exponentially decaying amplitude. A frequency analysis of the BC acceleration responses reveals motion with two distinct natural frequencies of the test rig, f_{n1}=122 Hz and f_{n2}=194 Hz for all directions. The first natural frequency $f_{n1}=\omega_{n1}/2\pi$ gives the structural stiffness of K_{Sn}=8.9 MN/m with the mass of the BC M_{BC}=15.15 kg ($\omega_n=\sqrt{K_S/M_{BC}}$).

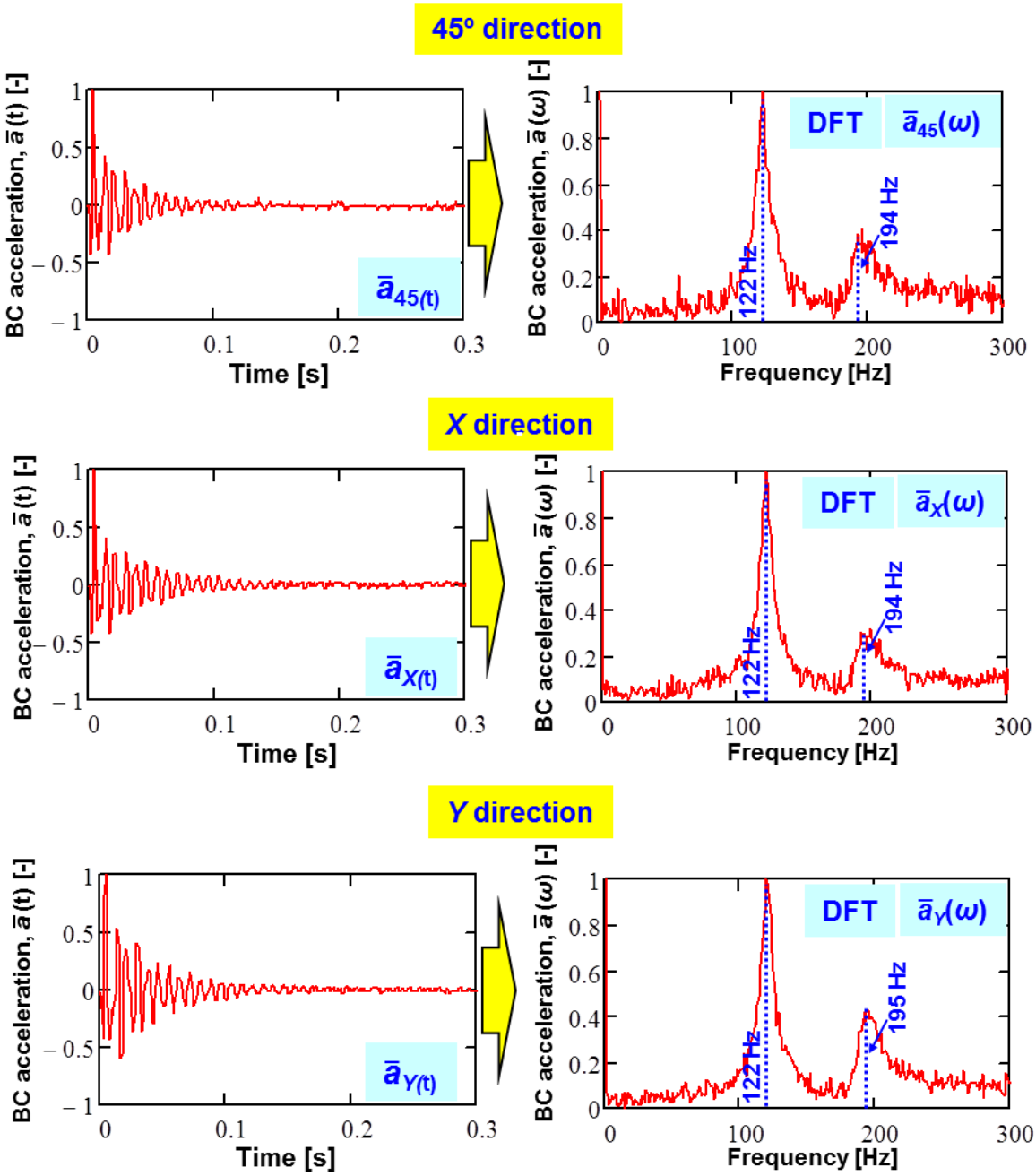

Figure A.2. Dimensionless BC acceleration ($\bar{a}$) and DFT of its amplitude for $\bar{a}$ versus time (t). Measurements for along the *X*, *Y* directions and 45° away at centered condition (e_s=0).

Appendix B. Measurement of test damper clearance

This section details the process used to calculate the radial clearance of current damper. Calculation of SFD radial clearance is:

$$c = \frac{1}{2}(D_{BC\_ID} - D_{J\_OD}) \quad \text{(B.1)}$$

where $\boldsymbol{D_{BC\_ID}}$ is the bearing cartridge inner diameter and $\boldsymbol{D_{J\_OD}}$ is the journal outer diameter. $\boldsymbol{D_{BC\_ID}}$ measurements were made with a dial bore gauge with measurement range of 1.27 mm (50 mil) and uncertainty of 1.27 μm (0.05 mil). The measurement of $\boldsymbol{D_{BC\_ID}}$ ~127.2 mm (~5.0065 in). Next, Figure B.1 summarizes the schematic view of the axial planes and angles used to investigate dimensions of $\boldsymbol{D_{J\_OD}}$.

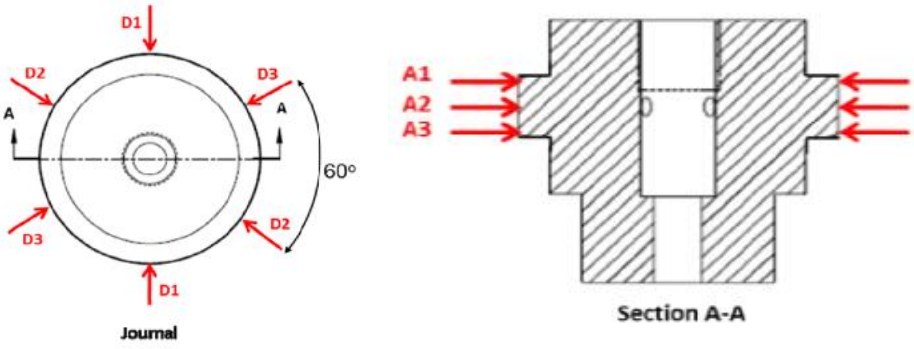

Figure B.1. Measurement planes for journal outer diameter (D planes are radial lines with constant spacing of 60º, section A-A shows axial planes spaced 12.7 mm (0.5 in) apart).

Table B.1 lists the average measured outer diameter of the journal at each plane, the BC inner diameter, and the average clearance. The average clearance is c=267 μm (10.54 mil).

Table B.1. Journal outer and BC inner diameter measured at three axial planes and three radial lines.

Measurement Plane	A-1 (Top) mm[in]	A-2 (Mid) mm [in]	A-3 (Bot) mm [in]
D1	126.6131 [4.98473]	126.6538 [4.98637]	126.6325 [4.98553]
D2	126.6165 [4.98490]	126.6436 [4.98597]	126.6233 [4.98517]
D3	126.6121 [4.98473]	126.6411 [4.98587]	126.6342 [4.98560]
Average	126.6137 [4.98479]	126.6462 [4.98607]	126.6299 [4.98543]
Total Journal OD Average:		126.6299 [4.98543]	mm [in]
Total Uncertainty: +/-		0.0025 [0.0001]	mm [in]

Average BC ID	127.1621 [5.0065]	mm [in]
Uncertainty: +/-	0.0025 [0.0001]	mm [in]

Average Clearance (*c*):	267 [10.54]	µm [mil]
Uncertainty: +/-	2.54 0.1	µm [mil]

Appendix C. Measurement of Lubricant Properties and Flow Rate

The oil, ISO VG 2 is routinely inspected, in particular the viscosity. At ambient temperature of 23^{o}C, the lubricant density is determined, by weighing a known volume of lubricant oil. The measured density is ρ=800 kg/m^{3}, in agreement with the manufacturer specifications, see Table C.1.

Table C.1. Mobil Velocite™ No 3 (ISO VG 2) Manufacturer specification [C1]

Mobil Velocite Oil Numbered Series No 3 (ISO VG 2)	
cSt @ 40℃	2.1
cSt @ 100℃	0.95
Pour Point, ℃	-36
Flash Point, ℃	84
Density @ 15° C, kg/L	0.802

Next, the lubricant dynamic viscosity is measured every three weeks and before/after rigorous testing as viscosity may fluctuate due to air ingestion, for example.

Figure C.1 shows the current and prior measurements of lubricant viscosity versus temperature along with the manufacturer specification. Presently, measurements give 2.4 cSt (1.92 cPoise, 0.281 micro-reyn) at 40℃ and 3.31 cSt (2.65 cPoise, 0.384 micro-reyn) at room temperature 23^{o}C. Note that the measured viscosity is different from the manufacturer specifications.

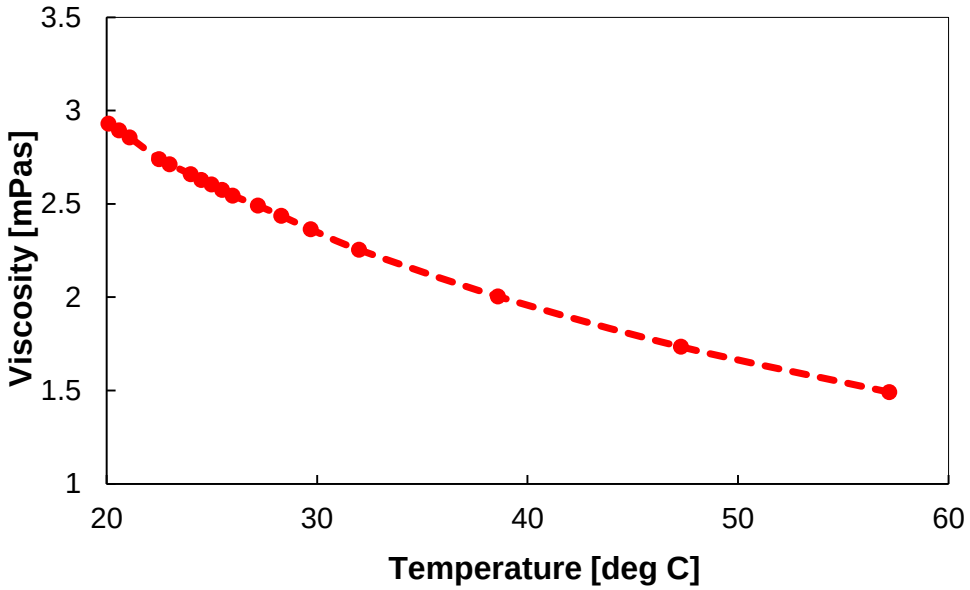

Figure C.1. Measured lubricant viscosity versus temperature. Viscosity measured with a rotary viscometer.

Measurements of flow through film lands

Lubricant is supplied at a user-determined supply pressure to the film land through three radial feed holes ϕ_{orif}=2.5 mm (0.1 in) and flows towards the top and bottom sections of the film land to ambient pressure. The lubricant inlet flow rate (Q_{in}) is measured by a turbine flow meter while a dial pressure gauge measures the inlet pressure (P_{in}) prior to entering the journal.

Table C.2 lists the recorded static pressures (P_{in}) and supplied flow rate (Q_{in}) for the damper. The flow conductance (C), the inverse of an hydraulic resistance (R), is derived from the supplied flow rate and the ensuing pressure drop across the film land and te orifices. P_a=0 (ambient).

$$\left[C_i = \frac{1}{R_i} = \frac{Q_i}{P_{in} - P_a} \right]_{(i=Total,B)} \tag{C.1}$$

The open ends SFD with c=267 μm (10.5 mil) and large diameter feedholes has a flow conductance C_{Total}=8.6 LPM/bar obtained from a linear regression of Q_{in} versus P_{in}, see Figure C.2. Note that the measurements point out to $Q_{in}(0) \neq 0$, indicating errors may exist in reading the pressure gauge and/or the turbine flow meter.

Table C.2. Open ends SFD (c=0.267 mm) with hex socket orifice, ϕ=2.54 mm. Measured inlet pressure and lubricant flow rate. ISO VG 2 oil at room temperature T_S=23°C [C2].

P_{in} (barg) [±0.003]	Q_{in} (LPM) [±5%]
0.19	3.10
0.32	4.58
0.46	5.98
0.63	7.19
0.81	8.52
Flow conductance	C_{Total}
LPM/bar	8.6

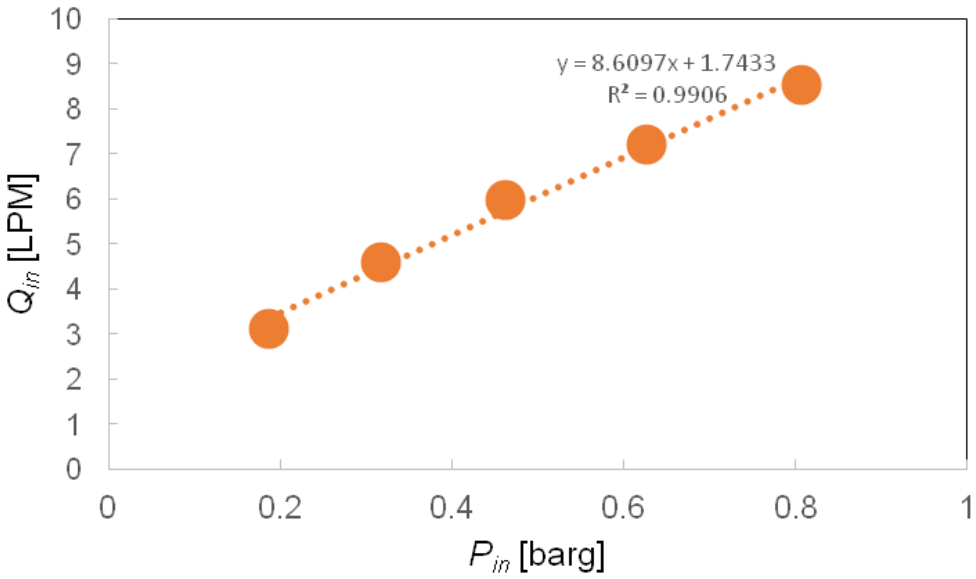

Figure C.2. Measured flow rate versus inlet pressure for journal with hex socket orifices ϕ=2.54 mm.

The theoretical flow conductance for an open ends short length SFD model without feed holes is

$$C_{land} = \frac{c^3 \pi D}{6 \mu L} = 115 \text{ (LPM/bar)} \qquad \text{(C.2)}$$

A large discrepancy is shown between the flow conductance from the test data and the one from a simple model not accounting for the feed holes. Lubricant supplied through the three orifice feed holes most likely increases the hydraulic resistance (R) and thus decreases the flow conductance (C=1/R).

The discrepancy in flow conductance indicates that the short length SFD model is not adequate for prediction of the SFD response.

References

[C1] "Mobil Velocite™ No 3 (ISO VG 2) Manufacturer specification sheet", Hydraulic oils Typical Properties, Mobil, Accessed October 2013, http://www.mobil.com/USAEnglish/Lubes/PDS/GLXXENINDMOMobil_Velocite_Oil_Numbered.aspx

[C2] San Andrés, L., Den, S., Jeung, S. H., 2014, "Analysis of Force Coefficients and Dynamic Pressures for a Short Length (L/D=0.2) Open Ends Squeeze Film Damper," 2014 Annual Report Report (Year VI) to Pratt and Whitney Engines, December.

Appendix D. Recorded Film Pressures in Test SFD[4]

This section presents an analysis of the film dynamic pressures as a function of the maximum BC displacement (Z) of the test damper.

Figure D.1 shows the position of pressure sensors in the bearing cartridge (BC). Eight piezoelectric dynamic pressure sensors (P_1 – P_8) are installed in the BC around its circumference. Two sets of three pressure sensors ($P_{1\text{-}3}$ – $P_{4\text{-}6}$), spaced apart by 90º, record the dynamic pressure at the top, bottom and mid sections of the damper land as shown in the figure. Note that $P_{1\text{-}2\text{-}3}$ and $P_{4\text{-}5\text{-}6}$ are spaced 15º apart. Two other piezoelectric pressure sensors (P_7 and P_8) measure the film dynamic pressures at the exit of the squeeze film land.

Figure D.2 compares the mid-plane ($P4$) pressure profiles for sudden impact loads, $F_{MAX}/(LD)$=3.9 bar, along Y direction and increasing static eccentricity e_s/c=0, 0.2, 0.4 and 0.6. The film pressure profiles resemble an oscillatory response with exponentially decaying amplitude that is similar to the responses of both the BC displacement. As with the observations from Figure 17, the magnitude of film pressure increases with static eccentricity, with the pressures at e_s/c=0.6 being significantly larger than the rest (notice the change in the vertical axis scale).

[4] Portions of this section reproduce ad-verbatim information presented in Ref. [21].

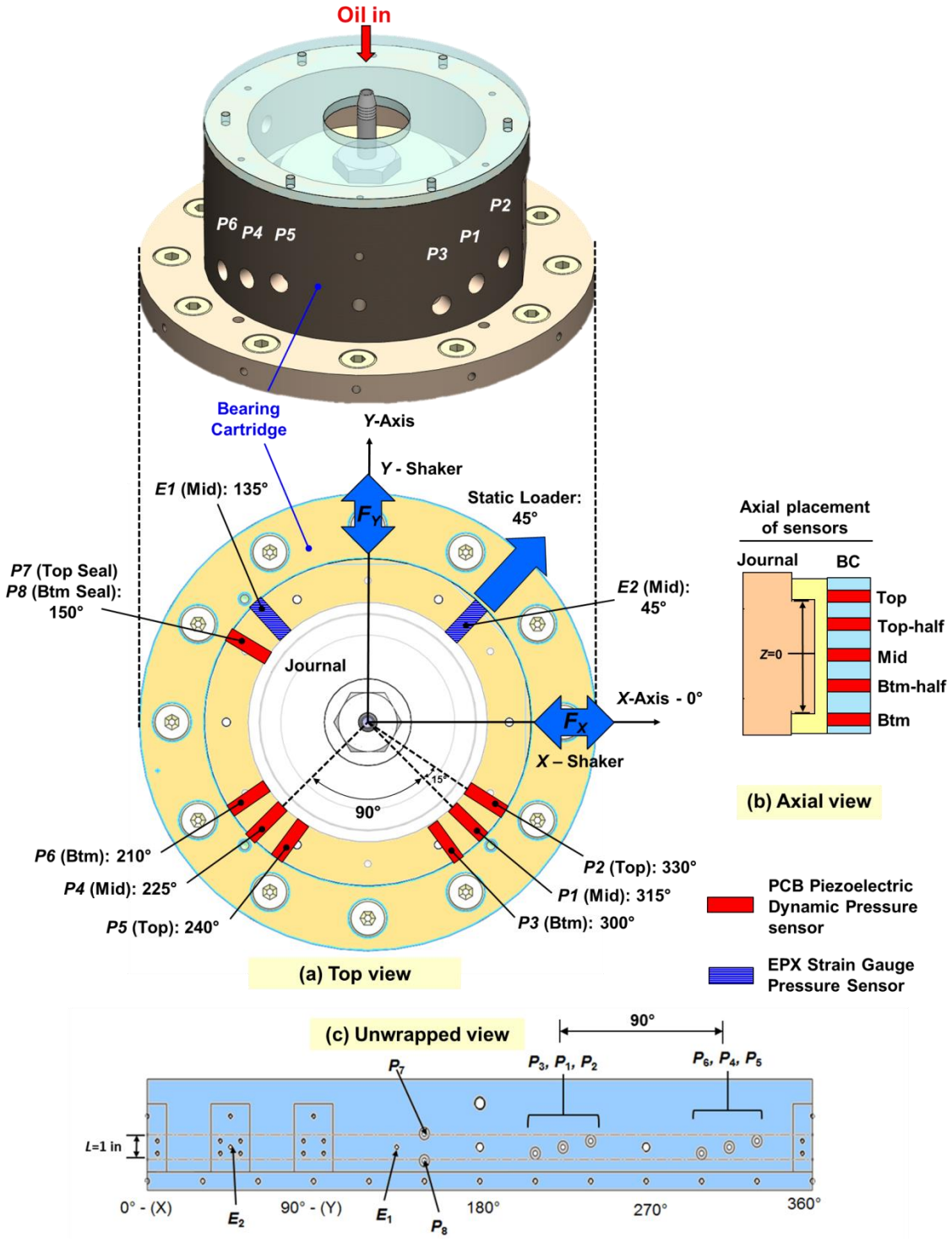

Figure D.1 Schematic views of the disposition of pressure sensors in the BC: (a) top view, (b) axial view and (c) unwrapped view [21].

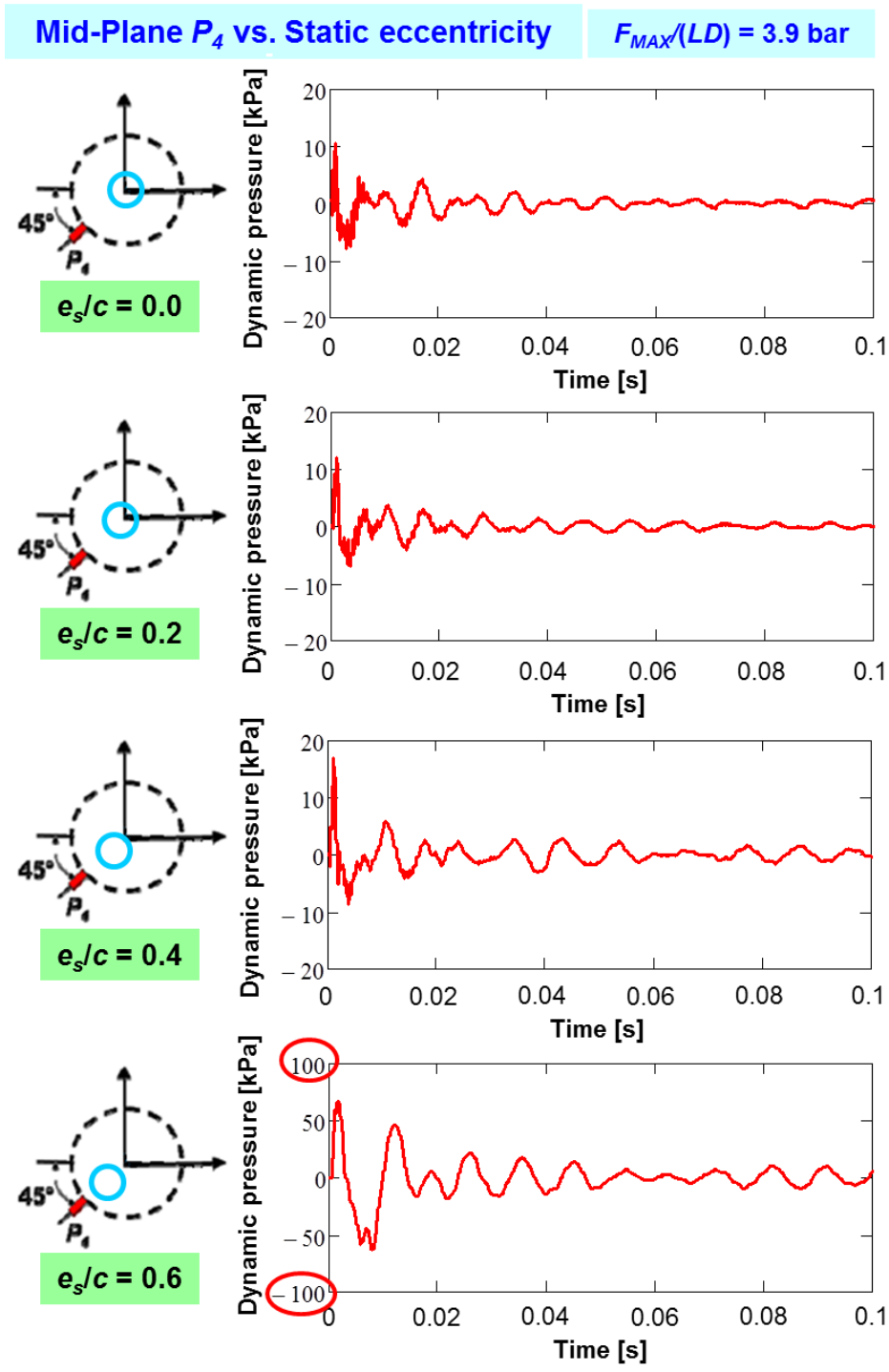

Figure D.2 Dynamic film pressures (*P4*) and film thickness (*h*) recorded at the mid-plane (*z*=0), and location of minimum film thickness for four static eccentricities. Unidirectional load along *Y* direction, $F_{MAX}/(LD)$=3.9 bar.

Figure D.3 presents the peak dynamic pressures for test damper versus peak unit load for motions for motions departing from (e_s/c=0) and static eccentricity e_s/c= 0.2, 0.4 and 0.6). The test data correspond to single impact load on the BC along the *Y* direction. An increase in peak BC displacement produces an increase in *p-p* dynamic film pressures. Expectedly, the top and bottom film pressures (z=±¼ L) are similar in magnitude; and at the mid-plane (z=0 L), pressures P_1 and P_4 are also similar in magnitude for motions from a small static eccentricity e_s/c<0.2.

However, for motions departing from a large static eccentricity e_s/c=0.6, see Figure D.3 (d), pressure P_4 is significantly larger than the film pressure at other locations (notice the change in the vertical axis magnitude). Recall the P_4 sensor is at the location of minimum film thickness (Θ=225°), opposite to the static eccentricity (e_s) displacement (Θ=45°, see insets on the left in Figure D.3). The comparisons between top and bottom *p-p* film pressures demonstrate that the top and bottom film lands are similar in operating film thickness and thus the bearing cartridge (BC) is properly aligned. For an open ends condition, the film pressures at the damper ends (z=±½ L) are nil.

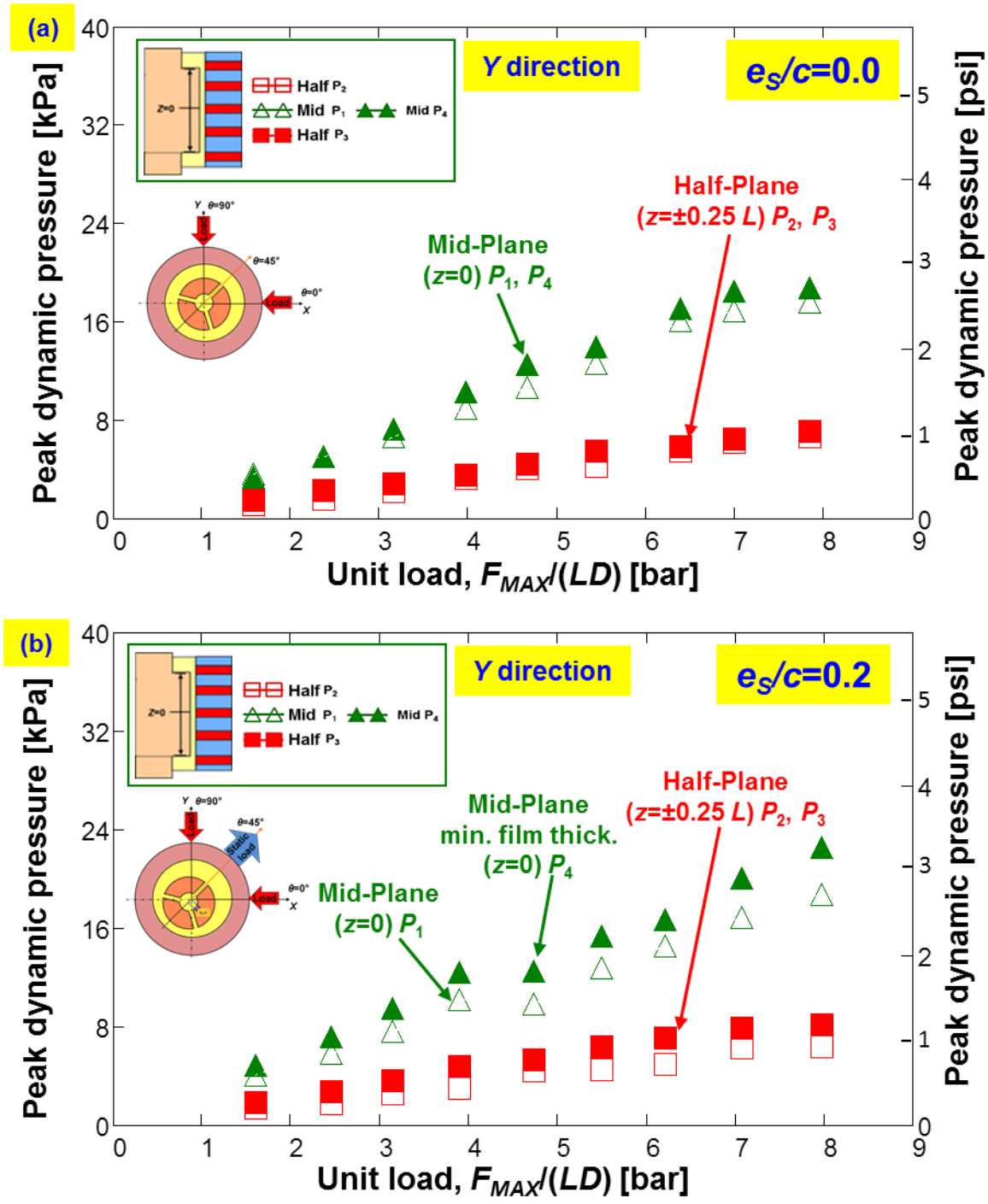

Figure D.3 Recorded peak film dynamic pressure versus maximum unit load $F_{MAX}/(LD)$ of single impact for motions from centered condition e_s/c=0 and three static eccentricity e_s/c=0.2, 0.4, and 0.6. Measurements at damper mid-plane, top and bottom half-planes. (Insets show location of pressure sensors along film land, and show journal position relative to the BC)**.**

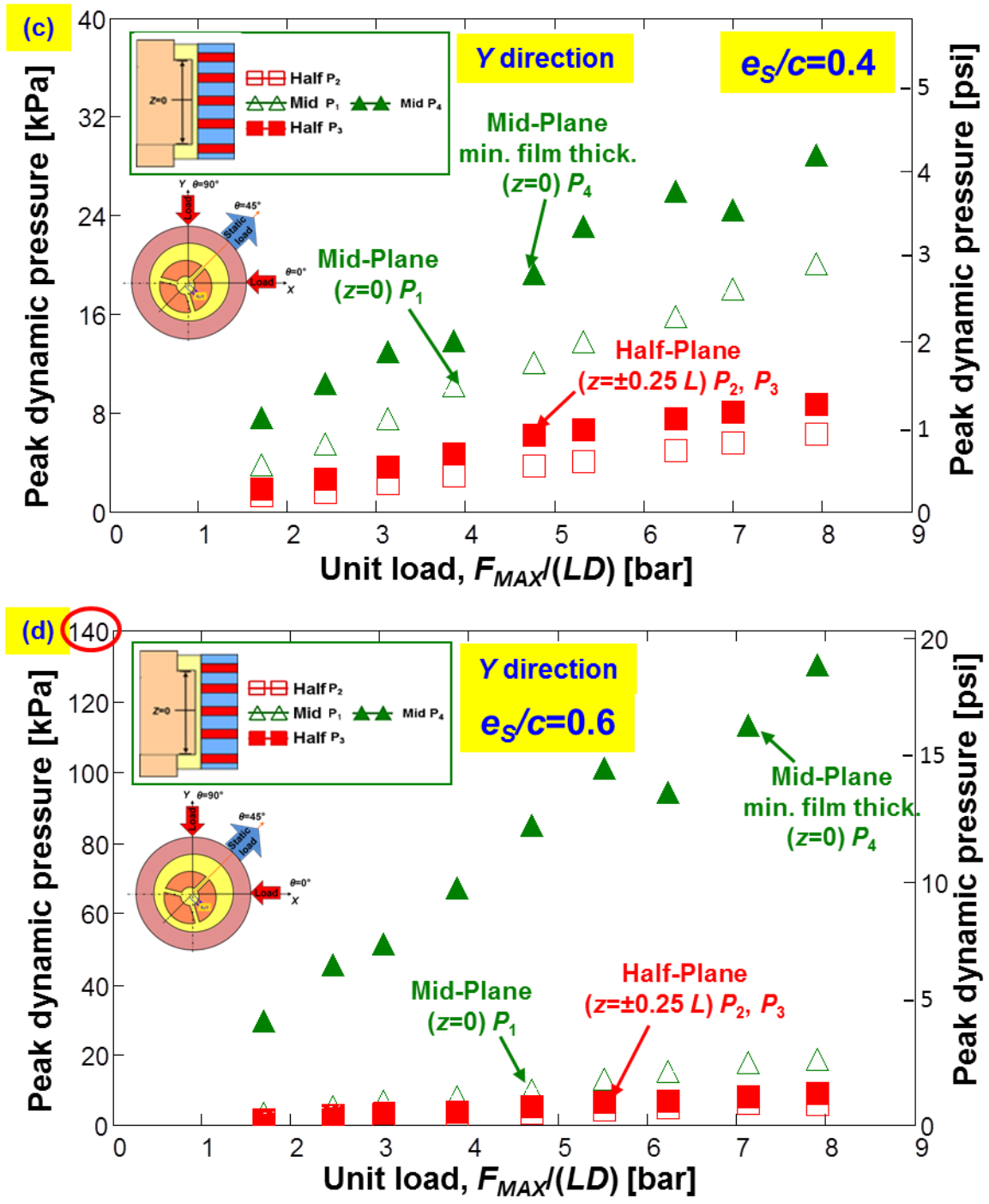

Figure D.3 Continued

Appendix E. Maximum displacement versus peak amplitude of impact load

Figures E.1 and E.2 depict the peak BC displacement ($|Z_{X,Y}|_{MAX}/c$) versus the peak amplitude of the impact load for four, five and six sequential impact loads, respectively. Insets on the top of the each figures show time trace of applied impact and ensuing BC displacement. Note that the maximum peak values are average over 20 test sets. The peak BC amplitudes tend to increase more with less unit load F_{MAX}/LD for the impacts following the initial one. For each impact, the change in slope of peak BC amplitude ($|Z_{X,Y}|_{MAX}/c$) over unit load (F_{MAX}/LD) is presented in Figure 11.

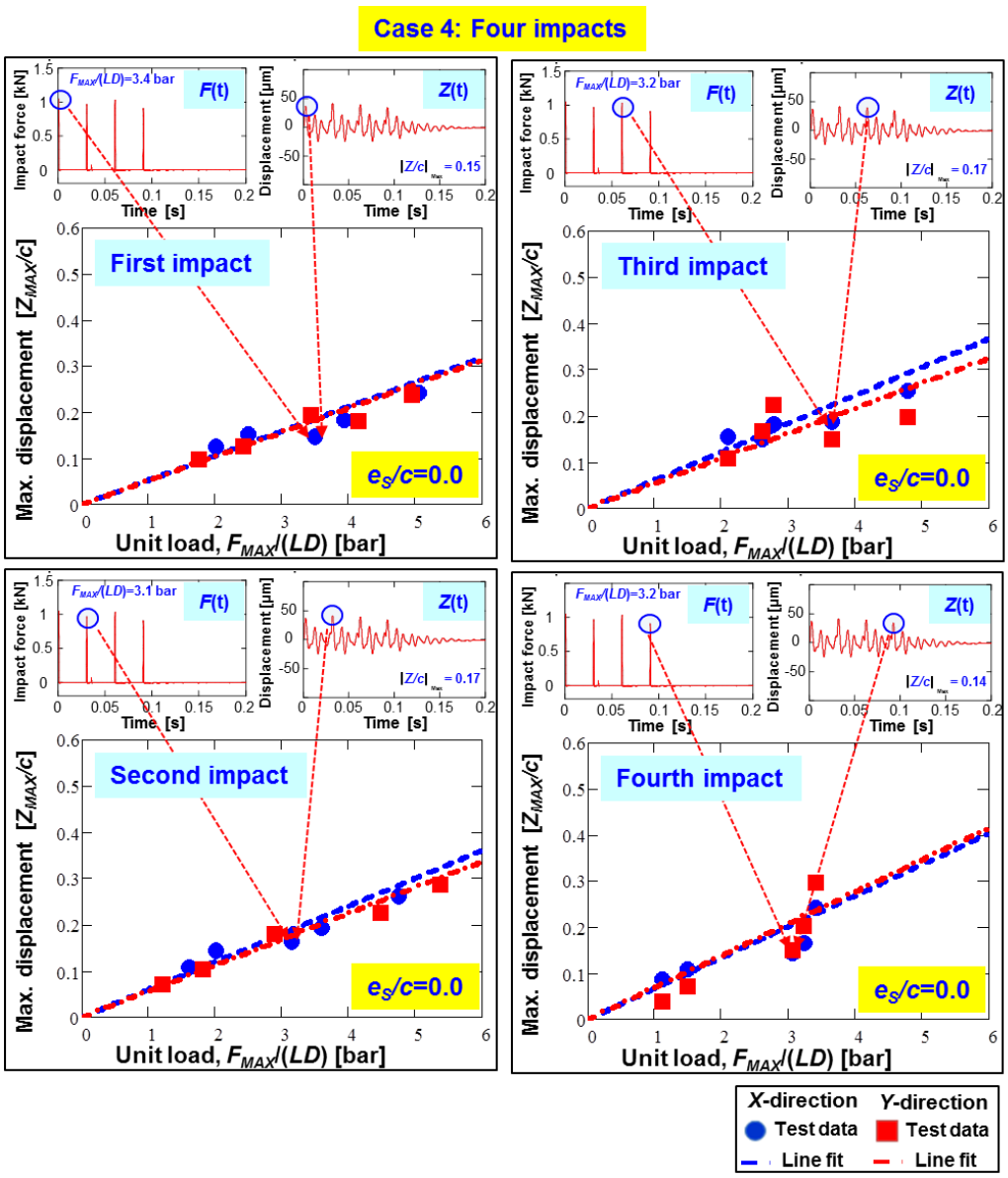

Figure E.1 Maximum displacement $|Z_{MAX}|_{X,Y}/c$ vs. peak amplitude of unit load $F_{MAX}/(LD)$ for motions from e_s/c=0 for four consecutive impact loads. Elapsed time between impacts T_i~30ms. Averaged over 20 test sets. Open ends SFD clearance c=0.267 mm. (Insets show time traces of impact load and ensuing BC displacement).

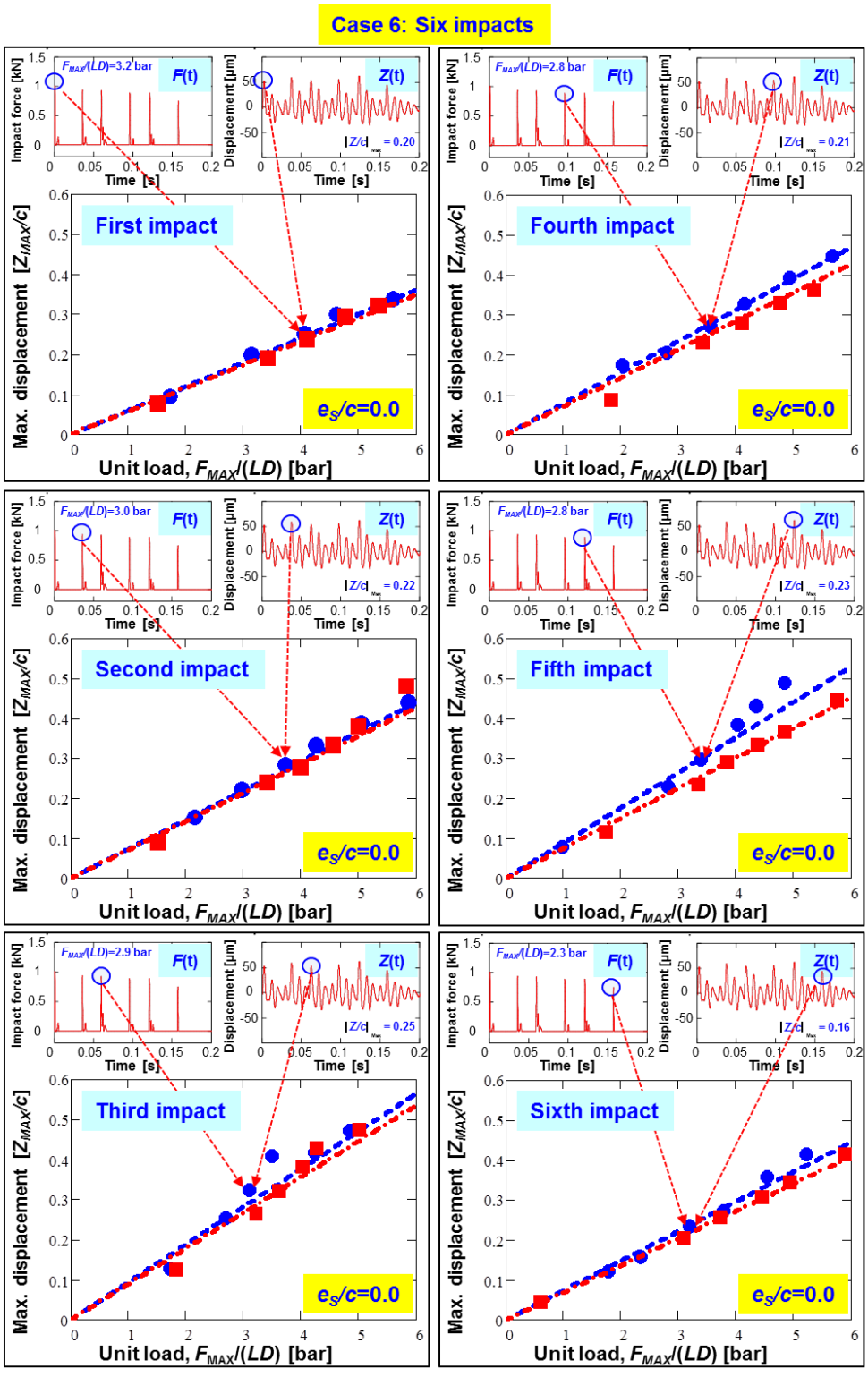

Figure E.2 Maximum displacement $|Z_{MAX}|_{X,Y}/c$ vs. peak amplitude of unit load $F_{MAX}/(LD)$ for motions from e_s/c=0 for six consecutive impact loads Elapsed time between impacts T_i~30ms. Averaged over 20 test sets. Open ends SFD clearance c=0.267 mm. (Insets show time traces of impact load and ensuing BC displacement).

Appendix F. Predicted Transient Response

Figure F.1 depicts the predicted response of the SFD for seven external impact loads applied to the journal. Note that the time of each impulse is ~1.4 ms and the elapsed time between impact is T_i =~30 ms. The time of the impact force correspond to external load of $F_{MAX}/(LD)$=1.6 bar, 3.1 bar and 6.3 bar for motions from e_s/c=0 centered condition (e_s=0).

Figure F.2 depicts the predicted peak BC displacement ($|Z_{X,Y}|_{MAX}/c$) versus the peak amplitude of the impact unit load ($F_{MAX}/(LD)$) for seven impact loads with T_i =~30 ms. Insets on the top of the each figures show the predicted time trace of applied impact and the ensuing BC displacement. For the impacts following the initial one, the peak BC amplitude tends to increase more with a reduction in load F_{MAX}.

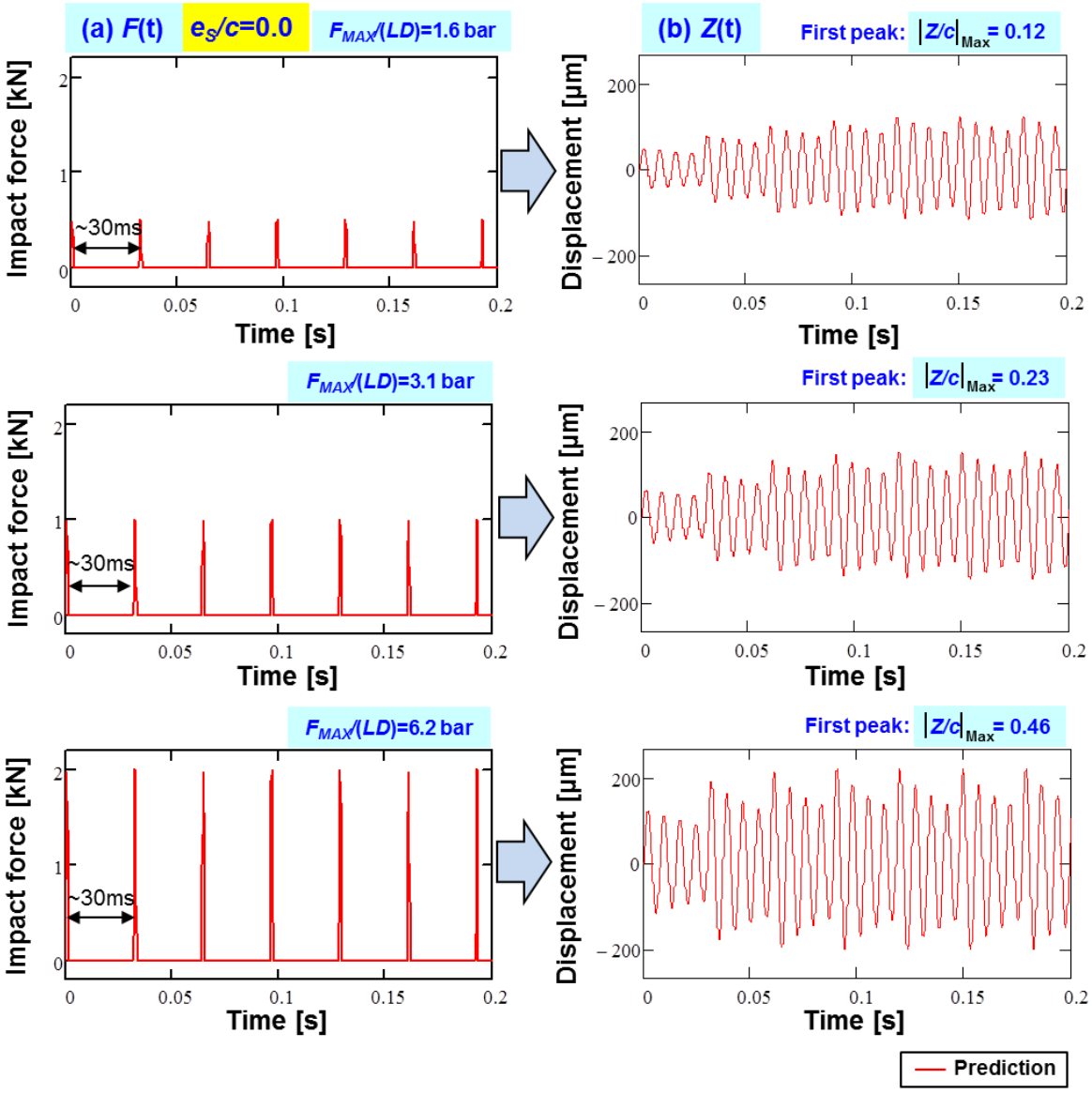

Figure F.1 Predictions: (a) Seven consecutive impact load *F*(t) and (b) calculated journal displacement *Z*(t) versus time. $F_{MAX\text{-}X}/(LD)$= 3.1 bar and motions from e_s/c=0. Elapsed time between impact T_i =~30 ms.

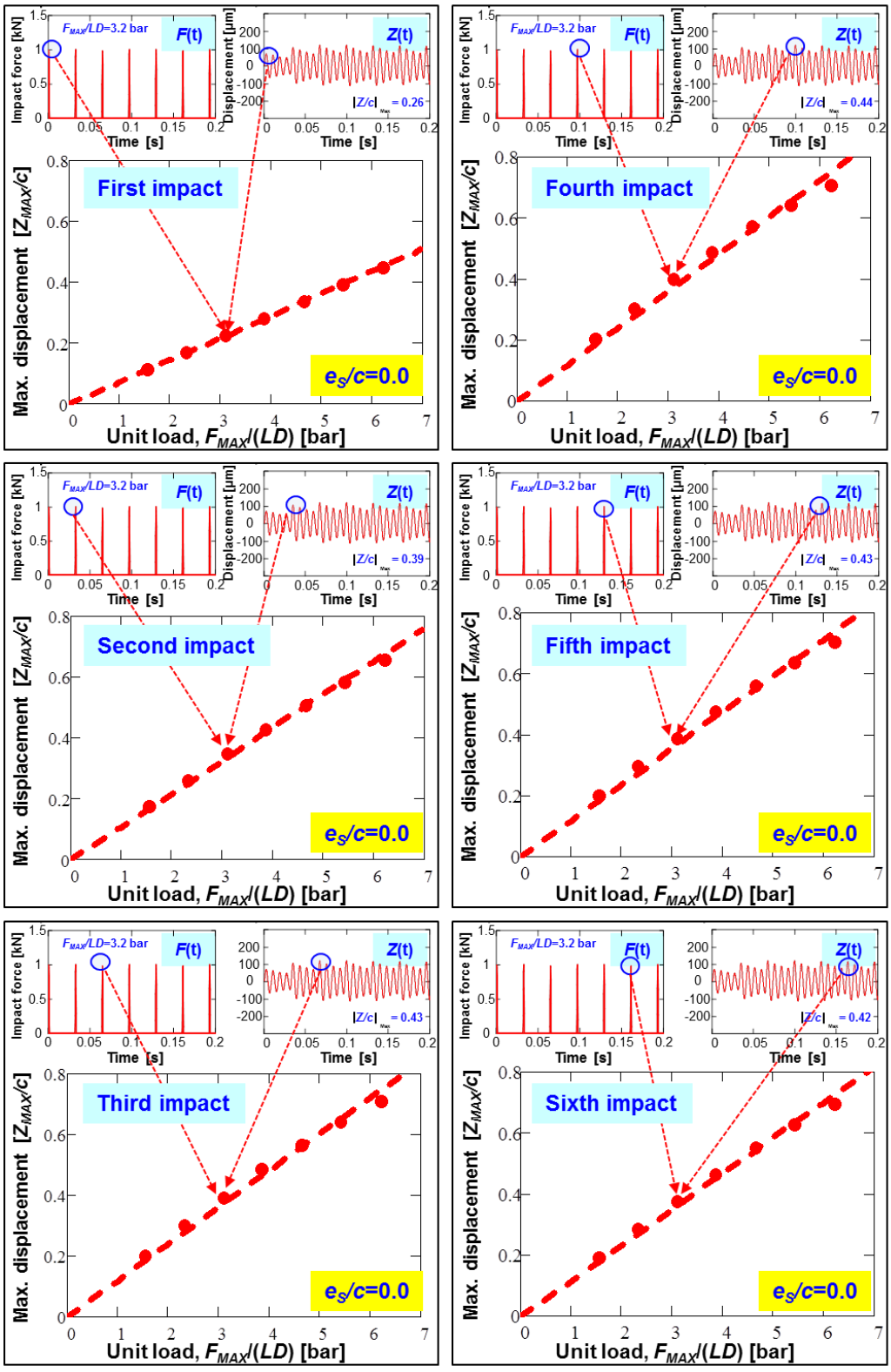

Figure F.2 Predicted maximum displacement $|Z_{MAX}|_{X,Y}/c$ vs. peak amplitude of impact load $F_{MAX}/(LD)$ for motions from e_s/c=0.